Printed Carbon Nanotube Electronics and Sensor Systems

*Kevin Chen, Wei Gao, Sam Emaminejad, Daisuke Kiriya, Hiroki Ota, Hnin Yin Yin Nyein, Kuniharu Takei, and Ali Javey**

Printing technologies offer large-area, high-throughput production capabilities for electronics and sensors on mechanically flexible substrates that can conformally cover different surfaces. These capabilities enable a wide range of new applications such as low-cost disposable electronics for health monitoring and wearables, extremely large format electronic displays, interactive wallpapers, and sensing arrays. Solution-processed carbon nanotubes have been shown to be a promising candidate for such printing processes, offering stable devices with high performance. Here, recent progress made in printed carbon nanotube electronics is discussed in terms of materials, processing, devices, and applications. Research challenges and opportunities moving forward from processing and system-level integration points of view are also discussed for enabling practical applications.

1. Introduction

Aligned with the vision of the Internet of Things, electronic sensors and systems are being seamlessly integrated in our surrounding objects at an exponentially increasing rate.[1] To promote this rate of integration, the development of printed flexible devices is critical, as their conformal nature and large-scale area of coverage meets the demanding mechanical and structural requirements imposed by emerging applications in various fields such as wearable electronics,[2,3] healthcare,[4] displays,[5] and human–machine interfaces.[6] Whereas state-of-the-art silicon-based integrated-circuit (IC) technologies are capable of implementing fast, energy efficient, miniaturized and low-cost computational systems, as achieved through the packing of transistors with increasingly high area density and reliability, they are not necessarily suitable for providing the sensing and actuation capabilities needed for flexible electronics and large-area applications. Conventional silicon IC chips are limited by the brittle nature of their silicon substrate, which prevents them from undergoing deformation and providing intimate contact with irregular surfaces. Moreover, the cost of production of IC devices scales in proportion to their area, and therefore the cost-effectiveness of this technology diminishes beyond a few square millimeters in area. Printable active flexible electronics are excellent candidates for facilitating large-area display,[5,7] sensing, and actuation functionalities. The unique capabilities offered by this class of electronics can particularly enable the development of a wide range of low cost mechanically flexible electronic platforms with active surface areas on the order of centimeters[8,9] to square meters,[10,11] as envisioned in **Figure 1**.[12] In this regard, printable platforms with active surface areas on the order of square centimeters are extremely low cost, while capable of providing numerous useful functionalities, and therefore are amenable for disposable applications, such as wearable electronics, food packaging, and medical devices. Moreover, printable flexible electronic platforms with active surface areas on the order of a few square meters or larger, which are implemented as a matrix of addressable and functional pixels,[5,8,13,14] fit well with applications requiring coverage of large surface areas with smart and interactive capabilities. In particular, such large-area platforms can be utilized in automotive, transportation, and human–machine interface applications.

From a system-level standpoint, realizing mechanically conformal, yet electronically advanced fully integrated platforms for the envisioned disposable and large-area applications necessitates devising solutions where printable flexible electronics and silicon IC technologies are synergistically combined in order to harness the unique capabilities offered by both technologies. In this regard, the two technologies may not be viewed as in competition, but rather as complementary with each other. Aligned with this vision, printable active flexible components fabricated on flexible substrates primarily serve as active devices to facilitate sensing, actuation, pixel control, and switching functionalities while directly interfacing the target surface areas that are on

K. Chen, Dr. W. Gao, Dr. S. Emaminejad, Dr. D. Kiriya, Dr. H. Ota, H. Y. Y. Nyein, Prof. K. Takei, Prof. A. Javey
Department of Electrical Engineering & Computer Sciences
University of California
Berkeley Berkeley, CA 94720, USA
E-mail: ajavey@berkeley.edu

K. Chen, Dr. W. Gao, Dr. S. Emaminejad, Dr. D. Kiriya, Dr. H. Ota, H. Y. Y. Nyein, Prof. K. Takei, Prof. A. Javey
Berkeley Sensor and Actuator Center
University of California
Berkeley Berkeley, CA 94720, USA

K. Chen, Dr. W. Gao, Dr. D. Kiriya, Dr. H. Ota, H. Y. Y. Nyein, Prof. K. Takei, Prof. A. Javey
Materials Sciences Division
Lawrence Berkeley National Laboratory
Berkeley, CA 94720, USA

Prof. K. Takei
Department of Physics and Electronics
Osaka Prefecture University
Sakai, Osaka 599–8531, Japan

DOI: 10.1002/adma.201504958

the order of square centimeters to square meters. To this end, advancements in thin-film materials have enabled development of processes that allow for the printing of physical, chemical, and optical sensors in an active-matrix format, where each pixel interfaces addressable integrated thin-film transistors[4,5] (TFTs). TFTs can be configured as sensing devices, as well as switch and decoder units for relaying control or transduced electrical signals.[15] TFTs can potentially serve as analog circuit elements,[16] as well to condition the transduced signal (e.g., through amplification and filtering) on-site, in order to preserve the signal integrity in the presence of electronic noise and other external sources of interference. Building on this approach, silicon IC components can complementarily be integrated onto flexible substrates to facilitate sophisticated signal conditioning, processing, and high-bandwidth wireless transmission; the functionalities that otherwise could not be realized through the sole use of printed flexible electronics. With this implementation, IC components are not constrained to and can be moved away from the sites of sensing and actuation prone to mechanical stress and deformation. Furthermore, the number of IC components is minimized, where only a single or a few IC components can meet the processing load of the whole matrix or a section of the matrix.

From a materials point of view, potential semiconductor materials for the target large-scale flexible and stretchable electronic applications include amorphous silicon, semiconducting metal oxides,[17,18] organic semiconductors, and carbon nanotubes.[5,7,10,19,20] While amorphous silicon-based devices have shown promising results in terms of achieving the target performance and have found use in commercial applications, they are not compatible with large-scale printing processes. Hence, they may not be a good fit for extremely low cost and large-area applications. Organic semiconductors can be printed using traditional printing processes such as inkjet printing and gravure.[21] However, they suffer from relatively low mobility and poor stability in air, making them less attractive for TFT applications,[2] although it should be noted that, for applications involving vertical transport rather than lateral, such as photodiodes and light-emitting diodes, where mobility is not as critical, organic semiconductors show excellent promise due to the tenability and broad range of materials available.[22] Semiconducting metal-oxides have been shown to be compatible with solution-based printing processes, as well as having very respectable mobilities.[18] However, while they can be engineered to perform reasonably well under bending, they may not be applicable to certain applications where stretchability may also be required. As such, the scope of this review is focused on the use of carbon nanotubes as the material of choice for flexible and stretchable electronic systems, with an emphasis on their use in TFTs for pixel addressing units for large-area applications. Carbon-nanotube networks have been shown to be resilient to deformation and can realign themselves upon experiencing large amounts of strain,[23,24] making them excellent candidates for use as electrical interconnects,[25,26] electrodes,[22,27] and the channel material for TFTs[4,19,24] in flexible and stretchable applications. It has been demonstrated that solution-processed, semiconductor-enriched CNTs have high mobilities, which enables high current drives at low operating voltages.[16,28] Simple deposition methods such as drop-casting[29] and spin-coating[20] also make these nanotube networks compatible with high-throughput printing processes.

For the rest of this manuscript, in Section 2 we present the growth, purification, and assembly processing strategies used to print CNT samples. Then, in Section 3, low-cost printing methods amenable to medium and large-scale volume

Kevin Chen is currently a Ph.D candidate in electrical engineering at the University of California, Berkeley studying with Prof. Ali Javey. He was the recipient of the Robert Noyce Memorial Fellowship in Microelectronics in 2015. His research interests include flexible electronics and thin-film materials growth.

Wei Gao received his Ph.D. in Chemical Engineering at University of California, San Diego in 2014 (with Professor Joseph Wang) as a Jacobs Fellow and HHMI International Student Research Fellow. He is currently a postdoctoral fellow on wearable devices with Prof. Ali Javey at the University of California, Berkeley. His research interests include flexible electronics, biosensors, naonomachines, and nanomedicine.

Ali Javey received a Ph.D. degree in chemistry from Stanford University in 2005, and was a Junior Fellow of the Harvard Society of Fellows from 2005 to 2006. He then joined the faculty of the University of California at Berkeley where he is currently a professor of Electrical Engineering and Computer Sciences. He is also a faculty scientist at the Lawrence Berkeley National Laboratory where he serves as the program leader of Electronic Materials (E-Mat). He is the co-director of Berkeley Sensor and Actuator Center (BSAC), and Bay Area PV Consortium (BAPVC).

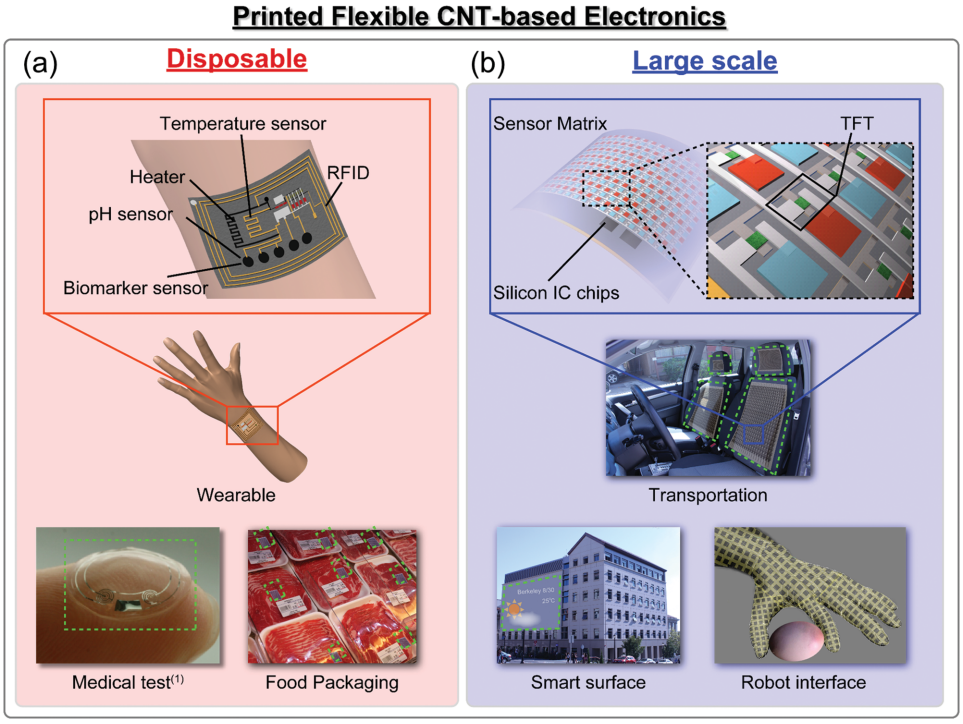

Figure 1. Overview of potential applications for printed flexible CNT-based electronics. a) Example applications of disposable, mass-produced flexible devices such as wearables, medical applications, and food packaging. Image (1) (Medical test): Adapted with permission.[12] Copyright 2012, IEEE. b) Example applications of large-scale integrated systems such as transportation, smart surfaces, and robotic interfaces.

production of flexible electronics are presented. In Section 4, we discuss the performance of printed CNT-based TFTs, and present demonstrated applications as enabled by the printed TFTs. In Section 5, we present the large-area systems that are realized through implementing addressable functional pixels. Finally, in Section 6, we provide an outlook in relation to the field of printed CNT-based flexible electronics and systems.

2. Processing

Since the report of multi-walled carbon nanotubes (MWCNTs) in 1991[30] and single-walled carbon nanotubes (SWCNTs) in 1993,[31,32] research on CNTs has been aggressively extended.[33–35] CNTs are allotropes of carbon consisting of single or multiple graphene sheets rolled up into a cylindrical shape. Single nanotubes can exhibit ballistic transport with current levels of up to 25 μA per tube[36] with high tensile strengths greater than 100 GPa.[37] Stimulated from their high performance and small feature sizes, CNTs have gathered tremendous attention as a promising materials platform for nanoelectronic device applications. In addition, the development of synthesis methods with high production yield has allowed the production capacity of CNTs to increase by more than 10-fold in the last decade,[37] which further facilitates the wide-spread use of CNTs as a common electronic material. As we discuss in this review, one application in which CNTs have been explored is as a semiconducting ink for printed large-scale and consumable flexible electronic devices.[38–40]

The most common synthesis methods that have been developed for the growth of CNTs are pulsed-laser deposition (PLD), arc-discharge, and chemical vapor deposition (CVD).[35,41] PLD applies laser pulses to evaporate graphite with metal catalysts, while arc-discharge uses a high current passed between two graphite electrodes to vaporize the graphite. CVD growth methods are based on the pyrolysis of hydrocarbons, and the high-pressure carbon monoxide (HiPco) method in particular uses carbon monoxide (CO) as the source gas.[41] To use CNTs as an electronic device material, especially as a channel material for thin-film transistor applications, the distribution of CNT sizes is critical for both device performance and uniformity.[42] SWCNTs can show both metallic and semiconducting behavior depending on their chirality,[42,43] which refers to the direction in which they are "rolled up" from a single-graphene sheet. Unfortunately, in almost all CNT growth processes to date, a wide spread of diameters is obtained, leading to CNTs with a variety of electronic properties ranging from metallic to semiconducting. To prevent leakage paths and improve uniformity within high-performance TFT devices based on SWCNTs, it is critical to be able to separate the different chiralities to reduce variation in the bandgaps of the SWCNTs, and, in particular, to be able to remove metallic SWCNTs. Although growth methods have been improved dramatically such that it is possible to obtain certain amounts of selectivity,[44,45] their as-grown selectivities are still inadequate for many applications, and post-growth separation methods must be developed to further separate each chirality for uniform SWCNT TFT operation.

2.1. Solution-Based Purification of Carbon Nanotubes (CNTs)

Due to the large-area high-throughput nature of printed electronics, a large amount of SWCNTs must be purified for such applications. In this regard, a solution-based method is ideal, as they can be scalable and handled simply from sizes as small as a small laboratory flask up to dedicated chemical plants. The main challenge with the purification of SWCNTs lies in the fact that there are only minimal atomic-level structural differences between chiralities.[46] To solve this issue, methods have been developed to enhance the differences between SWCNT chiralities by individually wrapping them with organic surfactants, after which the composite organic/SWCNT complexes allow for feasible separation. Various organic chemicals have been examined ranging from surfactants like sodium dodecyl sulfate (SDS)[47,48] and sodium cholate (SC),[49,50] peptides (e.g., reversible cyclic peptide),[51] poly(ethylene glycol)-based biocompatible polymers (e.g., Pluronic),[52] π-conjugated molecules or polymers such as porphyrines,[53,54] pentacene-based molecules,[55] flavine,[56] fluorene-based polymers,[57,58] and DNA.[59,60] Separation methods that have been explored include selective extraction based on differences in solubility of each chirality,[51,53–55,57,58] density-gradient ultracentrifugation (DGU) to separate chiralities via density differences under strong centrifugation,[49,50,52,61] size-exclusion chromatography to discriminate sizes and lengths,[47,48,62] and ion-exchange (IEX) chromatography[59,60] with charged media to separate each charged organic/SWCNT complex. Separation of SWCNTs with narrow diameter distributions has been achieved by the DGU method, allowing for separation of metallic and semiconducting SWCNTs with over 99% semiconducting SWCNT purity[49,52] (**Figure 2**a). IEX processes can separate charged structures and ions using the interaction with charges displayed in a stationary phase,[46] and has been explored mainly with DNA-wrapped SWCNTs[59,60,63] with precise separation of over 12 chiralities of SWCNTs demonstrated.[59] Recently, gel chromatography with dextran-based size-exclusion gel media (Figure 2b) has achieved large-scale (liter-scale) (Figure 2c) separation of up to 13 major chiralities of SWCNTs[48] with SDS as an organic support.[48,64] Currently, metallic and semiconducting enriched SWCNT powders and solutions are commercially available, although to enable the use of such SWCNTs as a material for printed electronics with large-scale and disposable applications, the cost and throughput of the purification methods must be further improved.

2.2. Solution-Based Assembly of SWCNTs

With the development of metallic and semiconducting enriched SWCNT solutions, the next challenge is regarding the effective assembly of SWCNTs onto various substrates from a solution.[65] In particular for device applications, the density of the nanotubes must be higher than the percolation limit in order to enable current conduction.[66] For solution deposition of CNTs, it has been found that the interaction between the organic CNT encapsulant and the substrate modification is critical to enable effective deposition. It was discovered that dense SWCNT networks can be obtained by spin-casting an organic 1-methyl-2-pyrrolidone (NMP) solution of SWCNTs onto a substrate modified with an amine (NH_2) moiety, which facilitates the assembly of SWCNTs to achieve a dense network.[20] As a result, TFTs with I_{on}/I_{off} ratios as high as 9×10^5 have been successfully demonstrated. In comparison, spin-casting the same solution onto a phenyl-moiety-modified substrate yielded a much sparser network. In addition to SWCNT assembly from organic solutions, assembly of SWCNT networks from aqueous solutions of purified SWCNTs has also been demonstrated onto a substrate with 3-aminopropyltriethoxysilane (APTES) modification.[29] The APTES-modified surface displays an amino-surface that enables significantly higher deposition yield as compared to deposition onto a non-APTES-modified surface. Using this solution procedure, wafer-scale uniform random networks of CNTs have been demonstrated. In addition to amine modification, pyridinium modification of substrates has also been demonstrated to enable deposition of SDS-wrapped SWCNTs with densities up to 10^9 cm^{-2}.[67] In this method, an SDS wrapped SWCNT is deposited onto HfO_2, which is modified with 4-(N-hydroxycarboxamido)-1-methylpyridinium iodide. The Coulombic interaction between the SO_3^- on the SDS/SWCNT complex and the N^+ on the pyridinium ions on the HfO_2 induces assembly of the SWCNT network. This method can be used to enable patterned deposition of SWCNT networks, as SWCNTs are only deposited onto pyridinium-ion-modified HfO_2 surfaces.

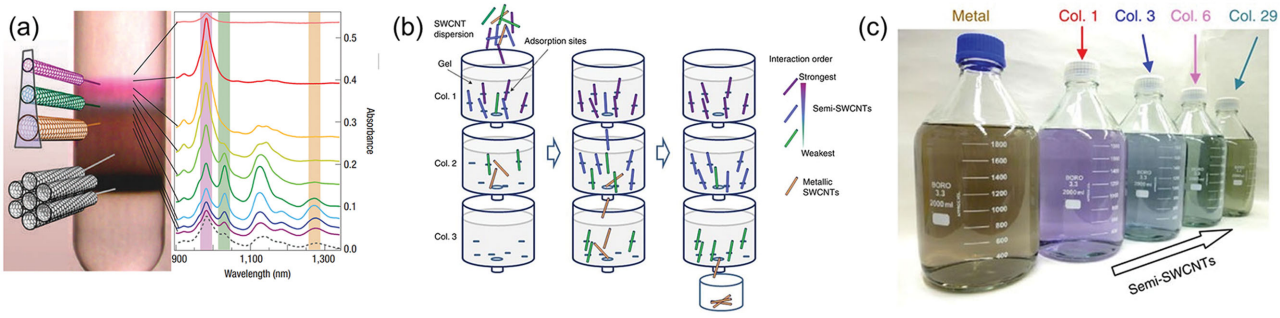

Figure 2. a) Purification using DGU with SC-wrapped SWCNTs. Different chiralities of CNTs are separated. Reproduced with permission.[49] Copyright 2006, Nature Publishing Group. b) Demonstration of large-scale purification by gel chromatography. c) Using the interaction between each chirality of SWCNTs and media, metallic and semiconducting SWCNTs can be separated with liter-scale throughputs. Reproduced with permission.[48] Copyright 2011, Nature Publishing Group.

In most solution-deposition-process schemes, the CNT assembly process typically takes on the order of tens of minutes to a few hours. However, to enable mass production of CNT-TFTs, particularly for compatibility with high-throughput roll-to-roll printing processes, it would be ideal to obtain dense CNT networks in less than a minute. To achieve this short deposition time, the interaction between the amine-modified substrates and surfactants on SWCNTs has been studied recently.[65] Commercially available semiconducting SWCNTs were first dispersed in several surfactants such as SDS, sodium dodecylbenzenesulfonate (SDBS), and SC, and were then deposited onto amine-modified substrates. Interestingly, only the steroid SC surfactant enabled dense SWCNT assembly on the substrate. It was discovered that, for the alkyl-chain based SDS and SDBS surfactants, the amine-modified surface induces assembly of a monolayer or bilayer structure, which eventually repels further assembly, leading to sparse or non-existent CNT networks (**Figure 3**a). On the other hand, it was shown that for steroid-moiety surfactants such as SC, while adhesion is promoted by the amine-modified surfaces, such mono-/bilayers do not form, leading to dense CNT network deposition (Figure 3b) with effective SWCNT coverages of up to 99%, estimated via capacitance–voltage measurements. In addition, percolating networks enabling TFT operation can be achieved within 60 s. Using this deposition procedure, a roll-to-roll assembly process of SWCNTs was demonstrated in which a 1 m-long poly(ethylene terephthalate) (PET) film was rolled through an SC encapsulated SWCNT solution, resulting in TFTs with an I_{on}/I_{off} as high as 10^3.

In the future, deposition times must be further improved for high-throughput printable processes and more research must be done to enhance the electronic properties of the deposited CNT networks. One example of such improvements in deposition method is the addition of mechanical shearing during the deposition process which results in aligned SWCNT networks with improved performance over random networks.[68]

3. Printing Methods

For the fabrication of functional flexible electronic devices using solution-processed CNTs, many researchers have traditionally used polyimide as the substrate of choice.[4,5,69,70] Due to its high temperature stability and the ability to be spun and cured onto a silicon wafer, polyimide allows for compatibility with many complementary metal-oxide-semiconductor (CMOS) processes such as photolithography and atomic layer deposition.[4,5] This compatibility enables the use of CNT-based flexible electronics in applications where fine pixel resolution

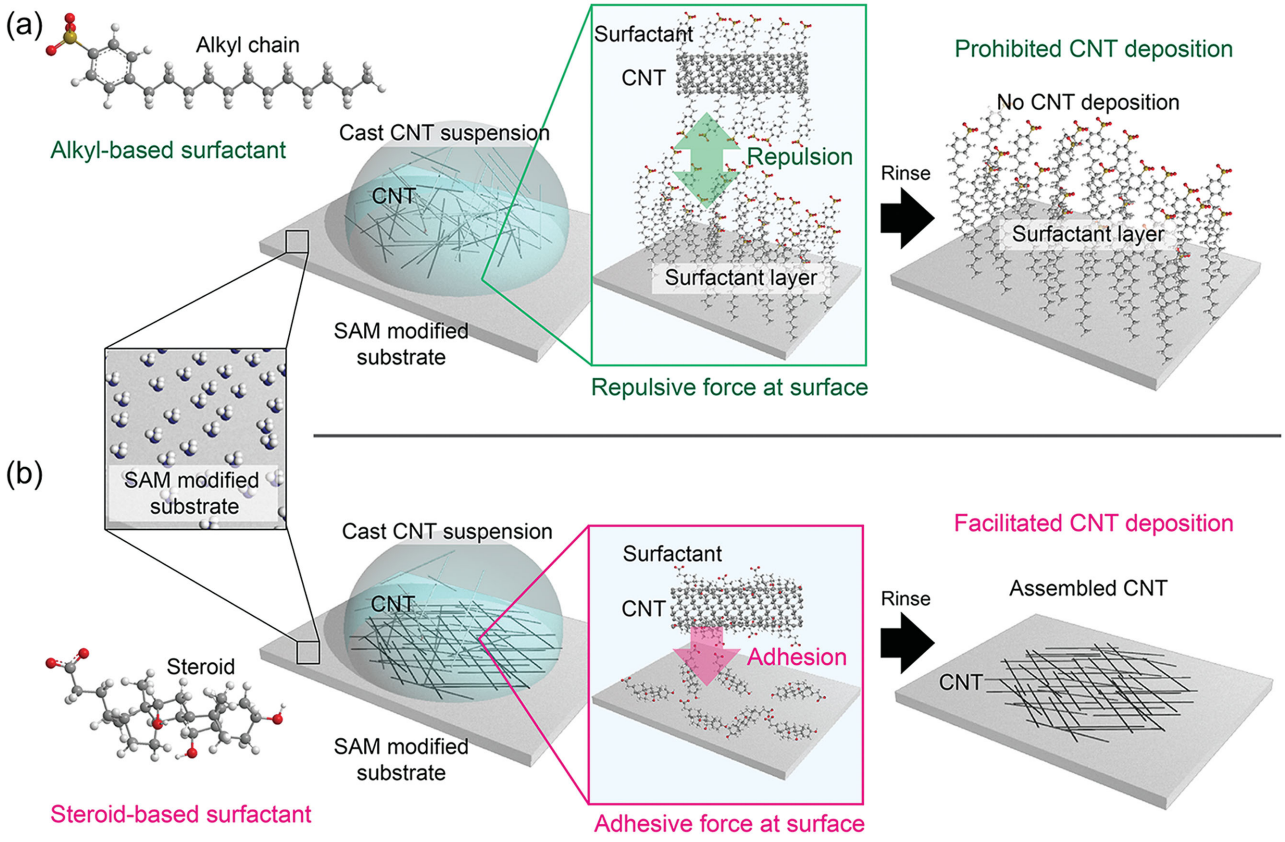

Figure 3. Illustrative image of the assembly mechanism of surfactant-wrapped SWCNTs on amine-modified substrates. a) The solution-based process from an alkyl-based solution of SWCNTs. Alkyl-chain-based surfactants are assembled onto the substrate, which prohibits the assembly of SWCNTs. b) The assembly process of SWCNTs from SC-based surfactant solutions. SWCNTs are assembled on the substrate via SC surfactants to form dense networks. Reproduced with permission.[65] Copyright 2014, American Chemical Society.

combined with high performance is desired. On the other hand, the ability to solution-process carbon nanotubes as the channel material in TFTs also enables CNT-TFTs to be compatible with a multitude of printing processes[8,19,71–73] for applications targeting large device areas that may be unfeasible using traditional CMOS technology from processing and cost perspectives. Printing is an attractive technology for many low-cost large-area applications as it removes many of the high-cost low-throughput processing steps found in traditional CMOS processing, such as lithographic patterning and vacuum processes for deposition of thin films. In addition, printed processes are highly compatible with flexible substrates such as paper[74] and polymers[71,73] unlike traditional CMOS processes which generally require rigid substrates in order to obtain fine feature sizes. Current commercial roll-to-roll printing processes are capable of printing at speeds of up to tens of meters per second,[75] and much progress has been made in recent years to obtain similar levels of throughput for the printing of functional electronics.

3.1. Inkjet Printing

One popular printing method that has been used for CNT-TFT fabrication is inkjet printing,[72,76–78] which is capable of printing a variety of functional inks including semiconducting, conducting, and insulating materials.[79,80] In inkjet printing, as shown in **Figure 4**a,[72] the desired ink is pumped through a nozzle with a diameter of tens of micrometers onto the substrate. Typically, inks are formulated with viscosities on the order of 1–20 centipoise (cp),[81] similar to that of water, so as to maintain good jettability of the inks. Using either a single or few inkjet nozzles, such as those found in personal inkjet printers, or up to hundreds of nozzles for commercial tools, inkjet printers are able to print fine features with picoliter-level droplet resolutions, corresponding to feature sizes as small as a few micrometers.[80]

Using inkjet printing, high-performance CNT-based TFTs with mobilities above 20 $cm^2\ V^{-1}\ s^{-1}$[72] and cutoff frequencies in the gigahertz range[76] have been demonstrated and configured as circuit components such as inverters, NAND gates, and ring oscillators.[72] The greatest advantage of inkjet printing of functional CNT-based electronics is probably its versatility in design. Due to the drop-by-drop-based printing method, inkjet printers are able to print any desired feature on demand within its resolution limits, making it an ideal solution for personalized electronics. In addition, a recent advancement made utilizing inkjet printing is the development of three-dimensional (3D) printing, where 3D structures may be fully printed utilizing a layer-by-layer inkjet-printing process.[82,83] This can potentially open the door for 3D-printed structures where functional electronic inks can be used to monolithically integrate printed CNT electronics within.

3.2. Roll-to-Roll Printing

Due to the serial printing nature of inkjet printing, it does suffer in terms of scalability and throughput as compared with other printing methods, while it is still much faster than traditional CMOS processes. In this regard, it may only be appropriate for application scales ranging from device prototyping up to medium-scale production throughputs. For extremely large scale, high-throughput applications, roll-to-roll printing methods may be more applicable. One such method that has been used for printing CNT-based electronics is gravure printing.[8,11,19,71] In gravure printing, the desired pattern is first engraved into a metal cylinder, which is then used to transfer the pattern continuously onto the desired substrate, analogous to the use of a photomask in lithographic patterning. Figure 4b[75] depicts the ink-transfer process for gravure printing. The engraved cylinder first rotates around an ink reservoir and then a doctor blade is used to remove any excess ink, ensuring that the only ink that remains is within the engraved cells. The engraved cylinder then rotates and transfers the patterned ink onto the substrate, passing along in the form of a continuous web on another cylinder. This process may be repeated multiple times to print the multiple layers of functional inks required in a high-throughput sequential process as depicted in Figure 4c.[11] Due to the continuous ink-transfer process, which does not require "stop and go" processing, roll-to-roll gravure printing, along with other similar methods such as offset or flexographic printing, can have throughputs on the order of meters per second

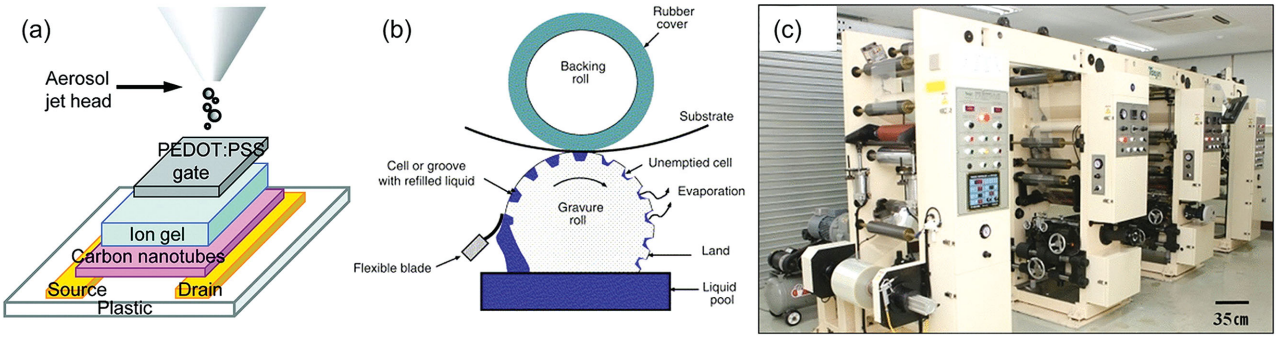

Figure 4. Printing processes for flexible CNT electronics. a) Schematic of the printing process for inkjet printing. Reproduced with permission.[72] Copyright 2010, American Chemical Society. b) Printing process flow of a gravure printer. Reproduced with permission.[75] Copyright 2006, Elsevier B.V. c) Optical image of a roll-to-roll gravure printer used for printed flexible CNT electronics. Reproduced with permission.[11] Copyright 2010, IEEE.

with resolutions of less than 5 μm,[21] making them ideal for large-scale commercial applications. As compared with inkjet printing, typical ink viscosities for gravure printing are on the order of ca. 40–2000 cP. As such, in order to directly print CNTs, a polymer binder matrix is typically required. However, the usage of a binder material to enable gravure printing of the active CNT layer will generally result in TFTs with lower performance.[10] An alternative method that has been proposed for the printing of CNT-based TFTs using gravure printing is to first deposit a blanket layer of CNTs across a full substrate, which can then be patterned and etched using oxygen plasma with a self-aligned process.[8,19,65] As roll-to-roll-compatible oxygen-plasma tools are commercially available, such a method would be able to preserve the high performance of solution-processed TFTs, while still allowing for compatibility with roll-to-roll processing. Using both printed and self-aligned deposition and etch processes for CNTs, it has been demonstrated that yields well over 95% can be achieved for printed CNT-TFTs via gravure printing[8,10] in academic-style laboratories.

One limitation of gravure printing is the need to create a new set of engraved cylinders for every design change. While the large capital startup costs of these cylinders can be averaged out when production scales are large, gravure printing may not be as suitable for prototyping or the production of small-scale flexible electronic systems where the large capital costs involved may not necessarily be recovered. In this regard, inkjet and gravure printing of flexible electronics can be viewed as complementary technologies which both merit further exploration to enable flexible and stretchable printed circuit applications for both smaller-scale personalized electronics as well as mass-produced large-scale applications.

4. Printed CNT-Based TFTs: Performance and Applications

4.1. Transistor Performance

Among printable channel materials for flexible TFTs, CNTs have been shown to have advantages in terms of performance and uniformity. Solution-deposited CNT-TFTs have been shown to have mobilities in excess of 100 $cm^2\ V^{-1}\ s^{-1}$,[28] with on/off ratios of up to 10^6. In addition, as mentioned previously, a unique aspect of CNT-based TFTs is the ease in which the electrical characteristics can be tuned by tuning the CNT density via the deposition parameters to fit different target applications.[84] For applications such as radio frequency identification (RFIDs), where high drive currents are necessary, a denser CNT network may be deposited in order to increase the maximum on current at the expense of a slightly increased off current. On the other hand, for applications such as flexible displays and imagers, where their dark levels/lower range of detection are limited by the off currents of the TFTs, shorter deposition times may be used to obtain higher on/off ratios. While utilizing a fully printed process may lead to slightly decreased performances as compared to lithography and vacuum-based processes due to materials and processing restrictions, the performance of fully printed CNT-TFTs can still reach mobilities as high as 9 $cm^2\ V^{-1}\ s^{-1}$ with on/off ratios of up to 10^6.[19] **Figure 5**a and 5b respectively show example images of a fully printed CNT-TFT array, printed via inverse plate-to-roll gravure printing, and a zoomed-in image of a single TFT within the array.[19] The TFTs utilize solution-deposited SWCNTs for the channel, as well as printed silver nanoparticle source/drain and gate lines and a printed barium titanate (BTO) nanoparticle-based gate dielectric. Figure 5c shows example transfer characteristics of over 60 fully printed CNT-TFTs within the array and Figure 5d and 5e respectively show histograms of the spread of on/off current ratio and mobility of the transistors. To demonstrate the robustness of the printed CNTs to strain, Figure 5f displays the transfer characteristics of a single TFT, which does not change even after 1000 bending cycles. While there is still device-to-device variation, especially in the off current and threshold voltage, it is adequate for many applications, such as use for pixel readouts in active-matrix backplanes, which can benefit greatly from the scalability of such a printable process. In addition, further optimizations in the printing of the metal and insulator/dielectric layers in order to obtain more-suitable metal work functions and fewer interface traps may eventually lead to drastic improvements in printed SWCNT device performances.

For flexible and stretchable electronics, one key aspect is the ability to sustain large amounts of strain without degradation or failure of the active materials. As many target applications include wearable and conformal electronics, such devices may undergo constant strain and deformation during use. In this aspect, CNT-network films display significant amounts of resilience to deformation, making them excellent candidates for use as electrical interconnects and electrodes to enable flexibility and stretchability.[24–26,85] As such, it is possible to construct highly stretchable and deformable CNT-based electronic devices. As an example, TFTs utilizing semiconducting CNTs as the channel material and unsorted CNTs as the metal electrodes, along with a stretchable thermoplastic polyurethane (TPU) dielectric has been demonstrated on a TPU substrate.[24] Due to the mechanical durability of the CNTs and the TPU material, the TFTs are capable of withstanding over 100% strain and able to survive impacts of up to 75 kPa, and even puncturing of the TFT. Another advantage of all-CNT-based transistors, in addition to the aforementioned stretchability and flexibility, is that they can be made to be fully transparent by using them in conjunction with transparent conducting contacts and gate dielectrics,[70,86–88] which may be useful in certain applications such as transparent displays, smart windows, or defense applications where transparency and invisibility may be required.

4.2. Printed CNT-Based Circuits

For more-complex logic circuits, commercial silicon ICs may be integrated along with printed CNT-based flexible electronics due to their much more powerful processing capabilities. However, simple CNT-TFT-based circuits may be desirable in large-area devices for immediate data processing and amplification to maintain signal fidelity through to the IC chips and prevent

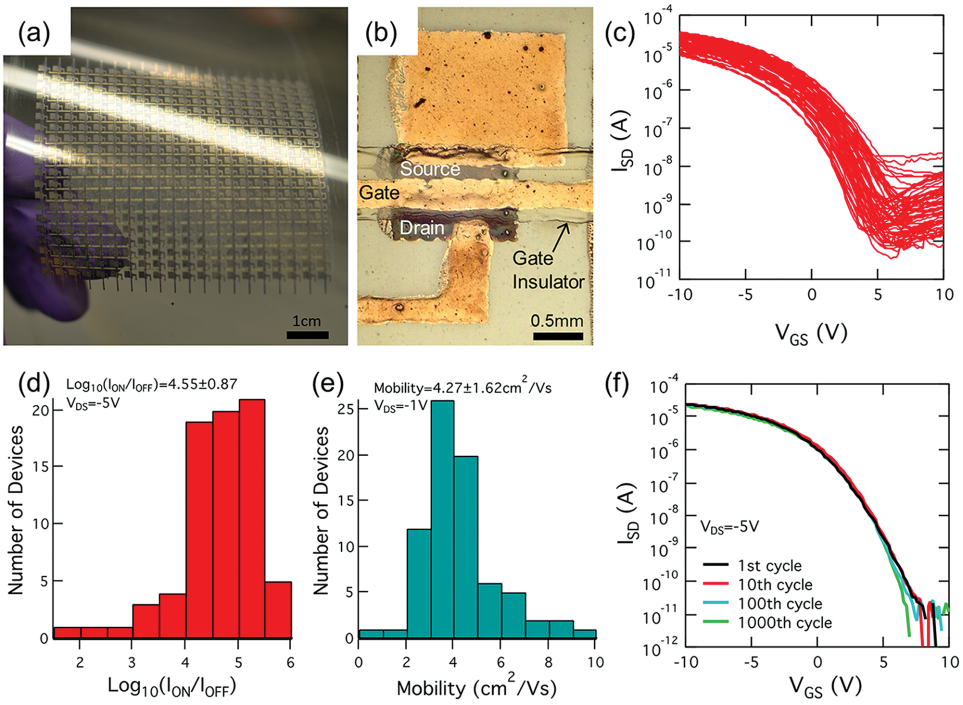

Figure 5. Performance of fully printed CNT-based thin-film transistors. a,b) Optical image of a 20 × 20 array of fully printed CNT transistors (a) along with a zoomed in optical image of a single TFT within the array (b). c) Plot of the transfer characteristics of 66 printed TFTs. d,e) Histograms of the I_{ON}/I_{OFF} ratio (d) and field-effect mobility (e). f) Transfer characteristics of a single TFT within the array after 1, 10, 100, and 1000 bending cycles. Reproduced with permission.[19] Copyright 2013, American Chemical Society.

signal decay. In addition, applications such as RFID tags and simple standalone flexible sensors may not require significant computational power, where printed CNT-TFT-based logic circuits alone may be sufficient. In this regard, many advances have been made in recent years to enable flexible CNT-based circuits with non-trivial complexity.

Among circuit components, the CMOS inverter is probably the simplest and most ubiquitous example for digital logic. From the performance characteristics of a CMOS inverter, the performance of other, more-complicated circuit components may be inferred. One main parameter of interest is the voltage gain of the inverter. Typically, a high voltage gain, corresponding to a steep transition from the on state to off state, allows for more-noise-tolerant circuitry, as well as lower voltage operation. In addition, a symmetric voltage-transfer curve (VTC), where the switching from a digital "1" to "0" occurs at approximately $V_{DD}/2$, is preferred so that the noise tolerance can be spread out between the switching behavior from both on-state to off-state and vice versa. For flexible electronics in particular, where devices may be required to operate in conditions with less passivation and shielding, as compared with traditional ICs, tolerance to noise is essential to prevent unintended switching within a circuit. In this regard, the relative strain-insensitivity of CNT-TFTs makes them ideal candidates for flexible circuit applications, as such circuits may need to operate while under various forms of deformation that may otherwise induce changes in transistor performance.

Intrinsically as-deposited, CNT-TFTs exhibit p-type behavior and, as such, much of the early work based on CNT-based inverters and circuits has been centered around p-type metal-oxide-semiconductor (PMOS) only logic. **Figure 6**a depicts an optical image of CNT-TFT-based circuits wrapped around a test tube.[16] Figure 6b and 6c display the performance of a PMOS-only inverter and a NAND gate, respectively, on the array, depicting a symmetric VTC curve and good rail-to-rail operation of the circuits. Using inkjet-printing technology, PMOS-only CNT-TFT circuit components, such as inverters and ring oscillators capable of operating at voltages of less than 3 V, have been demonstrated.[72] Figure 6d and 6e respectively show an optical image and the electrical performance of an example printed ring oscillator on a flexible polyimide substrate.[72] Printed PMOS CNT-based circuits such as D-flip-flops[73] and adders[89] have also been demonstrated via a roll-to-roll gravure-printing process. As an example of the complexity of computation that can be achieved on flexible substrates, a four-bit decoder consisting of 88 TFTs capable of operating at kilohertz frequencies has been demonstrated.[15]

One disadvantage of utilizing PMOS-only logic, however, is that even while not switching, current will still flow through the inverters, leading to constant power dissipation. Thus, it would be more ideal to be able to obtain n-type transistor behavior in CNT-TFTs to enable CMOS architectures for digital-circuit applications, so that the static power dissipation is limited only by the leakage current of the TFTs. To do so, various doping and electron-selective contact schemes have been proposed to enable n-type CNT-TFTs. Examples include use of remote fixed charges from thin-film oxides[90–92] and nitrides,[93] use of low-work-function metal contacts such as Sc[94] and Y,[95] and chem-

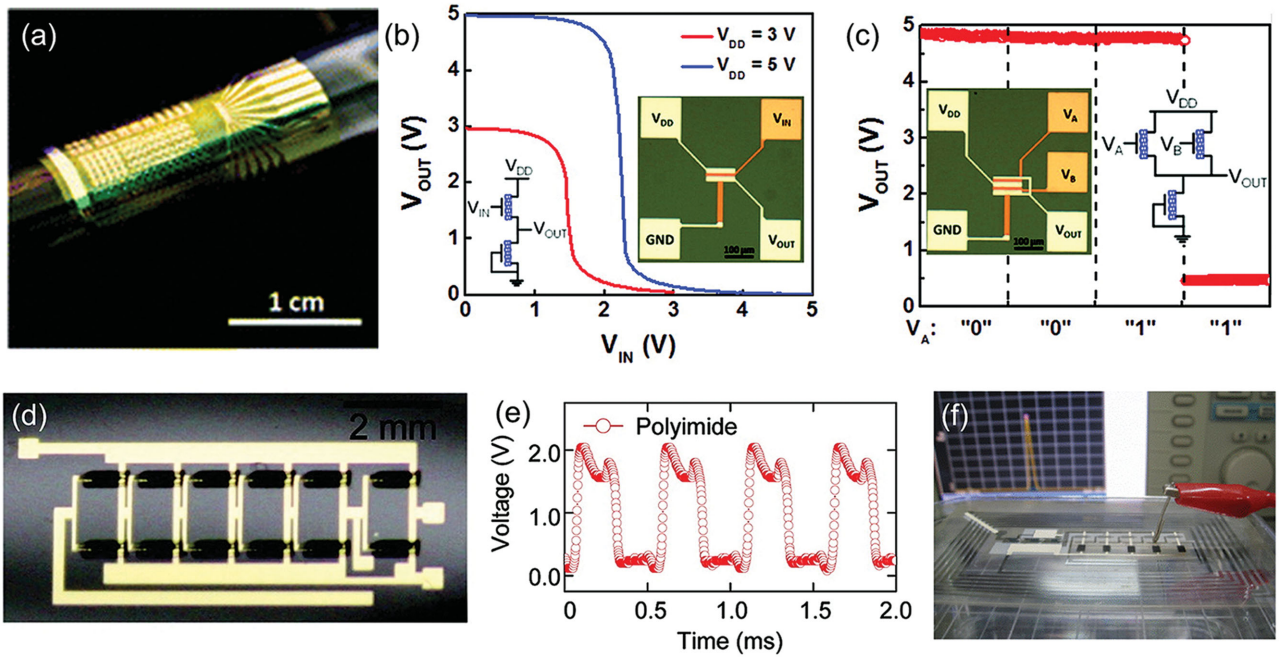

Figure 6. Printable CNT-based circuits. a) Optical image of a CNT-based circuit on polyimide wrapped around a test tube. b) Voltage-transfer characteristics of a CNT-based PMOS only inverter. c) Operation of a PMOS-only CNT-based NAND circuit. Reproduced with permission.[16] Copyright 2012, American Chemical Society. d,e) Optical image of an inkjet-printed five-stage CNT ring oscillator (d) and a graph displaying the switching behavior of the oscillator operating at a frequency of ca. 2 kHz (e). Reproduced with permission.[72] Copyright 2010, American Chemical Society. f) Optical image of a fully printed RF tag. Reproduced with permission.[71] Copyright 2010, IEEE.

ical doping with inorganic[96,97] and organic molecules.[69,98] While many of these proposed methods are able to induce n-type CNT-TFT behavior, it must be noted that they may not be compatible with printing-based processes, or may not have long-term air stability. For example, most oxide and nitride deposition methods require vacuum-based processes such as atomic-layer deposition (ALD) or plasma-enhanced chemical vapor deposition (PECVD), which are not possible to be integrated into a printed electronics platform. While materials based on metal oxides and nitrides may be utilized within a printed process,[18] experimental demonstration of utilizing such printed nanoparticles for doping of CNTs has not been demonstrated to date. Deposition of low-work-function contact metals also typically requires vacuum-based deposition processes in order to prevent oxidation of the metals, as it may not be possible to formulate printable inks with such low work functions. In terms of printability and stability, organic-based dopants could be more promising candidates.[69,98,99] For example, molecules based on dimethyl-dihydro-benzoimidazoles (DMBIs) have been shown to achieve tunable doping of CNT-TFTs via spin-coating and inkjet-printing processes.[69] Using these molecular dopants in an inkjet-printed platform, CNT-TFT-based CMOS inverters with gains of up to 85 V V^{-1} at a supply voltage of 80 V along with an impressive noise margin of 28 V, corresponding to 70% of ½V_{DD} can be achieved.

4.3. RF Applications

In addition to digital logic, radio-frequency (RF) applications may be advantageous for large-area flexible and stretchable electronics to provide wireless communications. The two important figures of merit for RF electronics are the cutoff frequency (f_t) and maximum oscillation frequency (f_{max}), corresponding to the highest frequencies at which the current gain and power gain of the transistor, respectively, are greater than unity. For long channel devices, the category into which most printed CNT transistors fall, the analytical expression for f_t can be written as:

$$f_t = \frac{g_m}{2\pi(C_{gs} + C_{gd})} \quad (1)$$

where g_m is the transconductance and C_{gs} and C_{gd} are the source and drain to gate parasitic capacitances, respectively. This indicates that, in order to obtain a good frequency response, a transistor should have a high transconductance with minimal parasitic capacitances. Due to the high mobilities of CNT network TFTs, they can have much higher transconductance values than organic semiconductor TFTs, making them more-ideal candidates for printed RF flexible electronics. In particular, as on/off ratios are not as critical for RF applications, as compared to digital electronics, higher cutoff frequencies can be gained in printed CNT-TFTs by simply increasing the CNT deposition time to increase the on current at the expense of increased off currents. As such, solution-processed CNT-TFTs capable of operating at frequencies greater than 1 GHz have been demonstrated,[76,100] with operational functionality maintained even when bent to radii of curvature as low as 3.3 mm.[100] As a potential application, RF tags, shown in Figure 6f, have been successfully printed

via gravure printing.[71] Such fully printed RF tags are able to operate at switching speeds of up to 100 Hz. It should be noted here that, typically, the cutoff frequencies of printed CNT RF circuits are lower than those of circuits fabricated via traditional photolithography. One major reason for this is due to the larger parasitic capacitances arising from the larger source/drain to gate metal overlaps. For future printed CNT-based flexible and stretchable RF circuit components, improvements in alignment accuracy and resolution along with development of self-aligned printing processes must be made to overcome these parasitic capacitances in order to achieve higher cutoff frequencies, as well as faster circuit operation.

4.4. Cyclic Voltammetry

Owing to their scalable manufacturability, printed CNT-TFT-based RF tags can serve as the key components for building disposable analytical tools at extremely low cost for chemical and biosensing applications. As an example, a disposable cyclic voltammetry (CV) tag has been demonstrated by combining basic electrochemical CV concepts with the wireless power-transmission capabilities of the printed RF tags[9] (**Figure 7**a). Figure 7b displays an optical image of a fully printed wireless cyclic-voltammetry tag. By taking advantage of the tunable properties of the CNT-deposition process, the performance of the drive, load, and buffer TFTs within the circuit can be optimized for higher current levels or higher on/off ratios. The printed CV tag operates wirelessly using a 13.56 MHz RF reader and generates a triangular sweep wave from –0.5 V to 0.5 V, which can be exploited to scan a printed electrochemical cell in the CV tag. As a demonstration, the presence of *N*,*N*,*N*′,*N*′-tetramethyl-p-phenylenediamine (TMPD) in the solution can be wirelessly and rapidly detected and shown on the signage of the CV tag within a few seconds (Figure 7c–f). This fully printed and wirelessly operated flexible CV tag opens the door to inexpensive and disposable wireless electrochemical sensor systems for the detection of a wide range of hazardous chemicals and biological species.

4.5. Chemical and Biological Sensing

In addition to their use as circuit components within a sensor or circuit array, carbon nanotubes are also an ideal material for chemical and biological sensors, as their extremely high surface-to-volume ratio makes them highly sensitive to changes in the surrounding environment. The transport behavior of the CNTs is very sensitive toward the local electrical field, which can induce charge redistribution in the CNTs.[101] This principle serves as the basic mechanism for designing sensitive chemical and biological sensors with CNTs. Sensors using printed CNTs as the active sensing element can be divided into several main categories: chemiresistive sensors, chemicapacitive sensors, chemical field-effect-transistor-based sensors, and electrochemical sensors.[2] Printed CNT-based sensors have been widely reported for the detection of a variety of chemical and biological analytes including hydrogen,[102–105] air pollutants (e.g., NH_3, NO_x, CO_x etc.),[106–110] organic vapors,[111,112] explosives,[113] nerve species,[114,115] and protein and DNA molecules.[116–118]

Sensing gas or organic vapor molecules is very important in environmental monitoring, chemical processing, healthcare, and agricultural applications.[119] Due to their high sensitivities, CNT-based devices have been demonstrated for use in monitoring environmental gases and organic vapors.[37] Early reported sensing devices are commonly made directly from pristine nonfunctionalized CNTs.[106,120,121] To add additional sensing capabilities, the CNTs may be functionalized with specific materials or receptors that can interact with the target molecules. **Figure 8**a illustrates a flexible hydrogen sensor fabricated with a printed thin film of CNTs decorated with palladium nanoparticles.[103] An optical image of a fabricated device with gold contact electrodes and a zoomed in atomic force microscopy (AFM) image of the Pd nanoparticles sitting on top of the CNTs are shown in Figure 8b and 8c, respectively. The palladium nanoparticles can actively react with hydrogen to form palladium hydride (PdH_x) at room temperature, and the variation in resistance of the CNTs caused by this reaction with hydrogen molecules provides the mechanism for fabricating sensitive hydrogen sensors. Figure 8d demonstrates the repeatability of the sensor response over multiple cycles to a hydrogen concentration of 500 ppm and Figure 8e displays the response of the sensor to concentrations of hydrogen ranging from 100 to 10 000 ppm. The detection limit for hydrogen sensing was found to be as low as ca. 30 ppm in air at room temperature. The sensitivity and response time of the sensor is plotted versus the hydrogen concentration in Figure 8f. As can be seen, the response time of the sensor decreases dramatically as the concentration increases. In addition, the sensing performance did not significantly change even after 1000 bending cycles.[103]

While CNTs are exceptionally sensitive to their ambient conditions and can be used to detect trace gas levels, a major flaw for such CNT-based gas sensors is their lack of selectivity.[99,120] To partially solve this problem, multiplexed sensing may be utilized. As an example, a flexible all-CNT electronic nose composed of one chemiresistive CNT sensor and one chemically sensitive CNT transistor has been demonstrated.[110] The chemiresistive CNT sensor utilizes CNTs functionalized with carboxylic groups (–COOH) and was able to detect CO with a detection limit down to 1 ppm. To distinguish the response to CO against other oxidative gases such as NO and NO_2, this chemiresistor was used in conjunction with a CNT-TFT fabricated using CNTs with no –COOH functionalization. As the CNT-TFT showed no response to CO due to the lack of –COOH functionalization, it could be used to adjust the response of the CO sensor to account for other oxidative gases.

In addition to gas sensing, printed CNT electronics on flexible substrates has also been demonstrated for the detection of a number of biomolecules and electrolytes.[117,122–125] Since the extremely small size of CNTs is comparable to those of biomacromolecules, they can serve as ultrasensitive transducers in biosensors. For example, a flexible and disposable immunosensor based on modified SWCNTs was demonstrated with a detection limit of 2.5×10^{-12} M for normal rabbit immunoglobulin G (IgG).[117] Printed CNT-TFT sensors using semiconductor-enriched SWCNTs have also been shown to be able to detect trace levels of analytes, such as dimethyl methylphosphonate

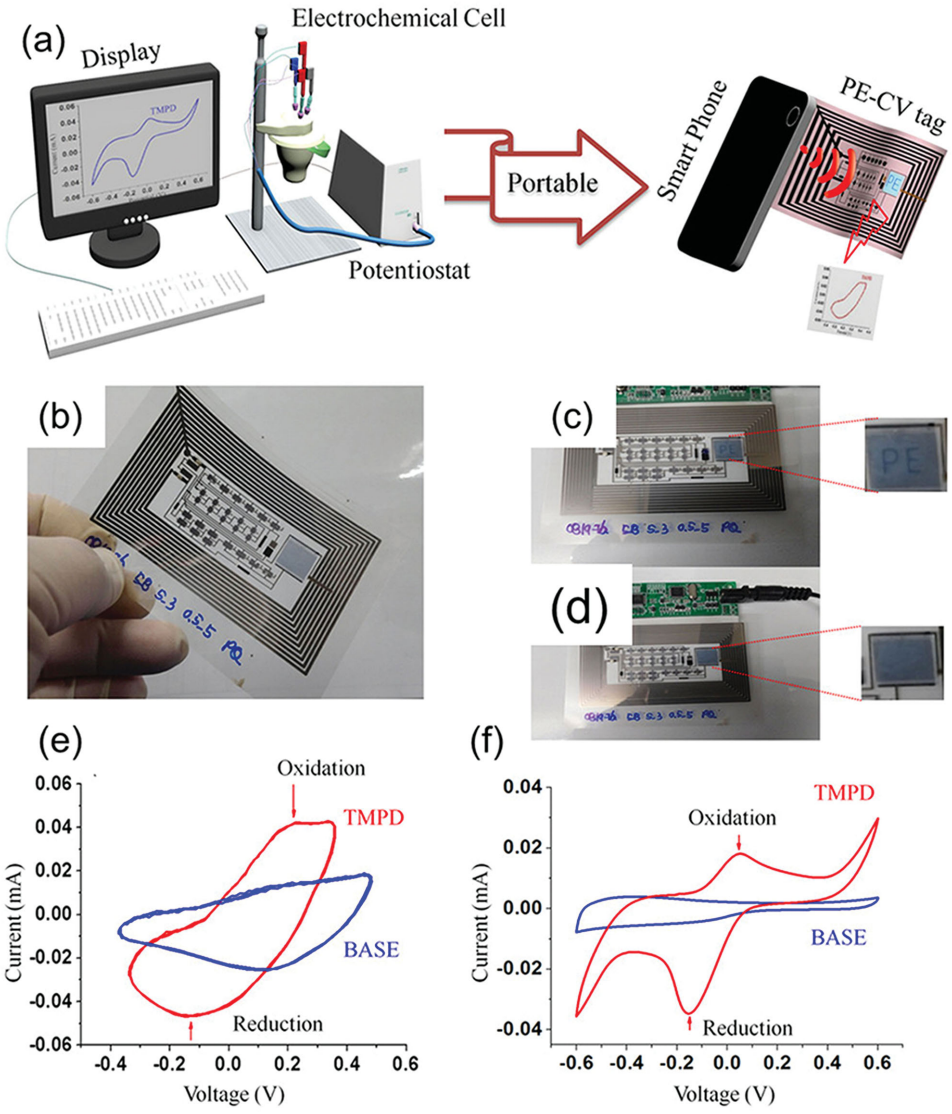

Figure 7. CNT-TFT-based cyclic-voltammetry system and disposable printed CV tag. a) Schematic illustrations of a typical CV system and disposable printed CV tag. b) Optical image of a fully printed wireless cyclic-voltammetry tag. c,d) Images of the CV tag during operation with (c) and without (d) TMPD in the solution. e,f) Converted cyclic voltammetry from the printed wireless CV tag (e) vs a commercial CV instrument (f) . Reproduced with permission.[9] Copyright 2015, Nature Publishing Group.

(DMMP) and trinitrotoluene (TNT), in aqueous solutions down to 2 ppb.[126] The usage of semiconductor-enriched SWCNT networks over unsorted SWCNT networks for the TFTs was shown to be critical in obtaining the high sensitivity level. However, similar to CNT-based gas sensors, CNT-based biological sensors show a lack of selectivity.

It has also been shown that for liquid-phase electrochemical detection of different analytes, printed CNT thin films have many advantages over traditional carbon electrodes such as larger surface areas, excellent charge-transfer promoting ability, and convenient protein immobilization for biosensors.[127,128] As such, significant advances in the development of CNT-based electrochemical sensors have also been made for the detection of a wide range of analytes such as glucose, H_2O_2, proteins, neurochemicals, and DNA.[117,129–133]

The previous discussion indicates that printed CNT thin films can serve as a promising candidate for future chemical and biological sensors where only limited selectivity is necessary. By using solution-deposition techniques for the CNTs, the fabrication process of these sensors can be easily altered to be compatible with facile and large-area fabrication approaches such as printed electronics. Although a variety of printed CNT-based flexible sensors with different functionalities have been demonstrated in recent years, most of the work so far has been focused on individual sensors; systems with multiplexed functionalities via integrating different types of devices along with commercial silicon IC chips for signal processing represent a major direction for future applications, especially for wearable electronic skins. In addition, further improvements in systems packaging along with sensitivity is also critically

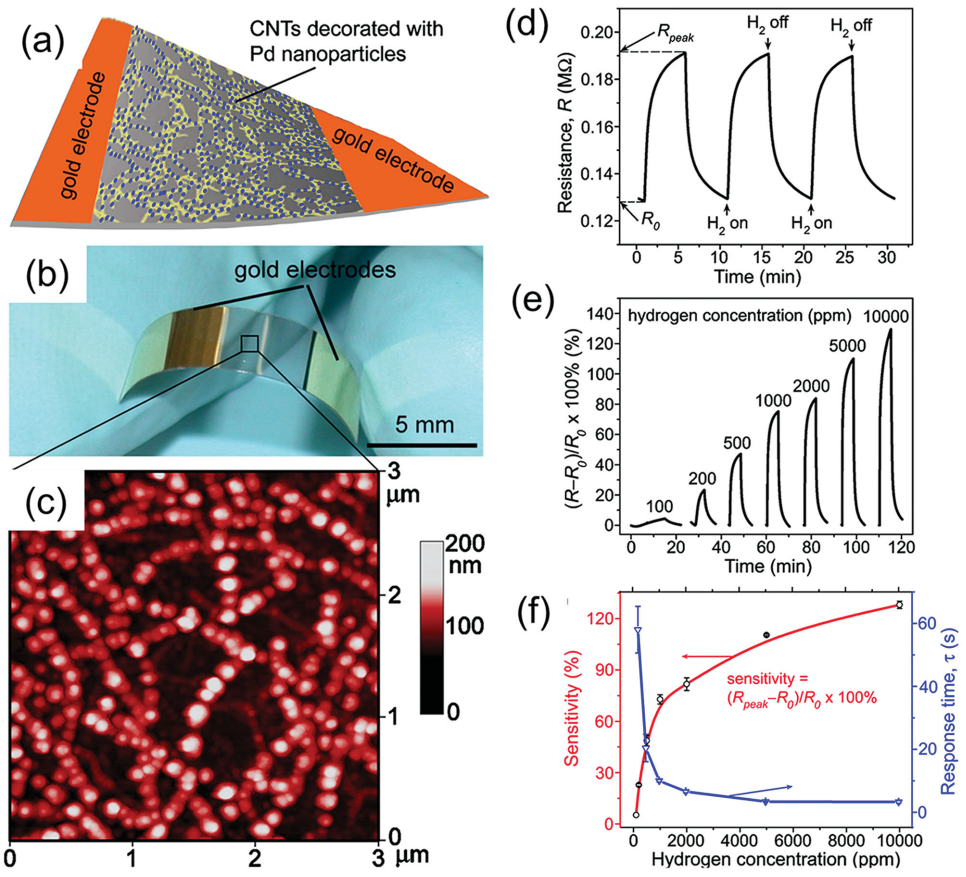

Figure 8. Pd nanoparticles (PdNP)-modified CNT thin film for hydrogen detection. a) Schematic of the flexible CNT hydrogen sensor on a PET substrate. b,c) Optical image of the fabricated sensor (b) and an AFM image of the Pd nanoparticles deposited on the CNT network (c). d) Response of the sensor to multiple exposures of 500 ppm of hydrogen, showing good repeatability. e) Response of the sensor to hydrogen at different concentrations. f) Plot of the sensitivity and response time of the hydrogen sensor versus the hydrogen concentration. Reproduced with permission.[103] Copyright 2007, American Institute of Physics.

important to obtain robust and reproducible devices as the response of the CNT-based electronics can be significantly influenced by changes in the ambient environment (humidity, temperature etc.).

5. Addressable Integrated Sensors and Displays

5.1. Fully Printed Backplane for Pressure Mapping

As discussed previously, one major advantage enabled by printable CNT electronics technology is the ability to scale up to ultralarge sizes on the meter-level scale and beyond for applications such as smart wallpapers, displays, or interactive surfaces. One key technology that is required for such scaling is the active-matrix backplane for the control of individual pixels within large arrays, which is most commonly seen in use for displays. In a simple active-matrix backplane, TFTs are arrayed into rows and columns, with all the drain lines within a given column tied together and all the gate lines within a given row tied together, or vice versa. Depending on the application, the source of the TFTs may be either connected in series to a sensor for sensing applications or a light-emitting diode (LED) for displays. The sensors may act as a variable resistor, with the final output current reflecting the amount of stimuli sensed. A universal ground is connected at the other end of all the sensors or LEDs to form a completed current path from which readings may be read out. Since both drain and gate lines must be active in order for current to flow in any given TFT, individual pixel control may be achieved in any arbitrarily large $m \times n$ array with an active matrix backplane using only $m + n$ control lines, significantly reducing the number of interconnects necessary, especially for very large arrays. From a design perspective, it is ideal for the on-state resistance of the TFTs to be as low as possible so that in the case of sensors, the resistance is limited by that of the sensor in series for maximum sensitivity or so that the maximum amount of drive current can be supplied to obtain higher brightness in display applications.

As a proof of concept, gravure printing has been utilized for the printing of a 20 × 20 array of CNT-TFTs in a pressure-sensor array for tactile pressure mapping.[8] Solution-processed CNTs were used as the channel material within the TFTs, while silver and BTO nanoparticle inks were used as the metal and dielectric layers, respectively. A yield of 97% was obtained for the 400 pixels within the array. For mapping functionality, pressure sensors in the form of a pressure-sensitive rubber (PSR)

were integrated into the array, contacting the source of each pixel on one side and a sheet of conductive carbon tape on the other, which acted as a universal ground. The PSR becomes more conductive as tactile pressure is applied, allowing for pressure sensing to be achieved. Mapping of the applied tactile pressure was successfully demonstrated by pressing a silicone "C" block onto the array, with higher current levels indicating applied pressure.

5.2. Flexible Displays

By integrating CNT-TFT active matrices with organic light-emitting diodes (OLEDs), flexible and transparent display applications can be achieved.[37] CNT-TFTs are particularly attractive for driving OLED displays because of their high mobilities, which can enable higher drive currents at lower operating voltages.[134] In addition, their ability to be deposited by low-temperature non-vacuum methods means that fabrication of such flexible displays may potentially be extended to printing-based processes. This can enable displays on a much larger size scale, as compared with current vacuum-based processes. As a proof of concept, printed TFTs have previously been successfully demonstrated for use in driving OLEDs. **Figure 9**a[78] depicts the output characteristics of a simple OLED driving circuit at different gate voltages using CNT-TFTs where the OLED is put in series with a single TFT. Figure 9b shows images of the OLED within such a circuit at different applied gate voltage biases, showing good modulation of light intensity. Due to the excellent transparency of CNT thin films arising from their extremely thin nature (typically a monolayer network), the driving circuitry for displays can also be made transparent by using SWCNT-based TFTs along with transparent conducting contacts and dielectrics, allowing for fully transparent displays to be achieved.[88] In addition to using semiconductor-enriched SWCNTs as a transparent TFT channel material, non-electronic-type enriched solution SWCNTs have also shown promise in display technology as a transparent anode material for OLEDs, as well as for transparent interconnects.[22,27,135]

In order to provide evidence for the practicality of employing CNT-TFTs in display applications beyond a single pixel, solution-processed CNT-TFT-based driving circuits can be arrayed in an active-matrix fashion and successfully exploited to control an array of OLEDs. Using a controlling circuit composed of two transistors per pixel, monolithically integrated active-matrix OLED (AMOLED) arrays with up to 500 pixels driven by 1000 CNT-TFTs have been demonstrated.[7]

As a further demonstration of complexity, pressure sensors can also be integrated onto a CNT-TFT active-matrix backplane in addition to OLEDs to achieve an interactive pressure-sensitive display. Figure 9c illustrates a schematic diagram of a single pixel within the interactive display.[5] Each pixel in the active matrix consists of a CNT-TFT with the drain connected to the anode of an OLED. The cathode of the OLED is then contacted by a PSR sheet, which is coated on the other side with silver ink as a universal ground. When pressure is applied to a certain region, the conductivity of the PSR within that region increases, allowing current to flow, and thus turning on the

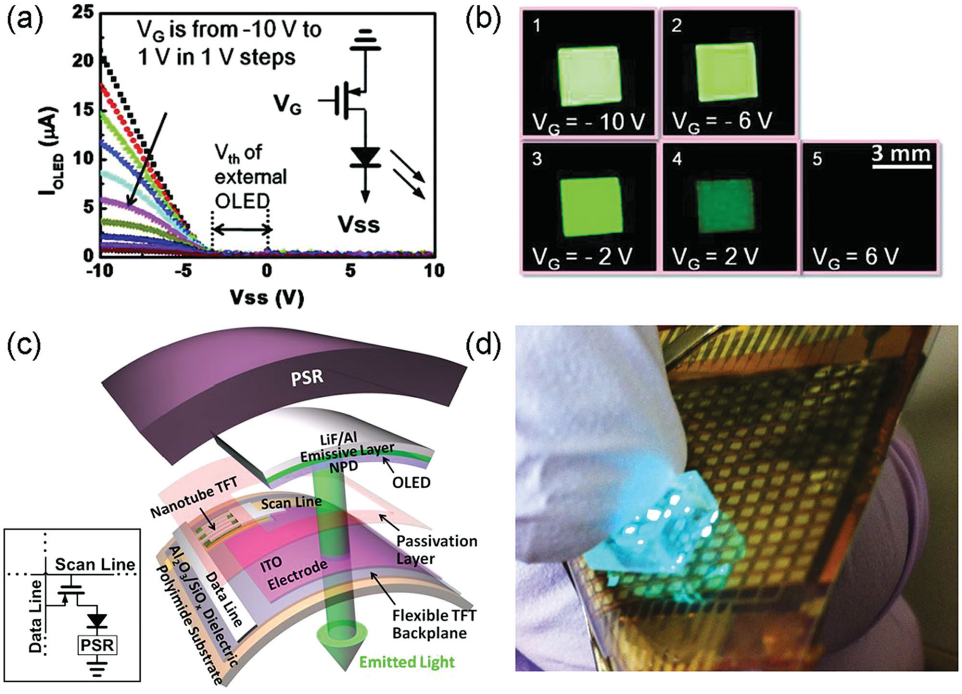

Figure 9. CNT-based TFTs for flexible displays. a) Output characteristics of a back-gated TFT connected to an external OLED. The inset shows the equivalent circuit diagram. b) Optical images showing OLED light-intensity modulation by the gate voltage of the back-gated SWCNT TFT at a supply voltage of 10 V. Reproduced with permission.[78] Copyright 2011, American Chemical Society. c) Schematic diagram of a pixel within a touch-sensitive OLED display with a CNT-TFT addressing unit. d) Demonstration of the interactive display that produces a light response where pressure is applied. Reproduced with permission.[5] Copyright 2013, Nature Publishing Group.

OLEDs controlled by the CNT-TFTs under the same area. As a proof of concept, the interactive display was exploited to spatially map and visually display the applied pressure profile (Figure 9d). This work provides an example of the compatibility of solution-processed CNTs with a large host of technologies to obtain heterogeneous integration of various electronic, sensor, and light-emitting components based on both organic and inorganic materials at a system level on thin plastic substrates.

In future work, CNT-based TFTs for display applications could involve enhancing the pixel yield and resolution, as well as improving the lifetime of the OLEDs. By exploring this implementation using a fully printed platform, sensor elements and OLED arrays could be explored toward extremely large scales.

5.3. Large-Area Imaging

Large-area flexible imaging represents another major application domain for CNT-TFTs. Their high mobility along with their high on/off ratios offers low-voltage operation with broad-range sensitivity, holding great promise for system-level, practical applications. By taking advantage of the excellent light absorption of organic bulk heterojunctions along with the excellent electrical properties of solution-processed CNTs, a visible-light and X-ray imager on flexible plastic substrates has been demonstrated by integrating solution-processed organic photodetectors on top of an active-matrix backplane based upon CNT-TFTs.[4] **Figure 10**a shows an optical image of a fully fabricated imager (18 × 18 pixels) placed on top of a Gd_2O_2S/Tb (GOS) scintillator film. The efficient light absorption of the organic bulk-heterojunctions provides high imaging sensitivity, while the high on/off ratio of the CNT-TFTs allows for broad-range detection. A log–log plot of the current as a function of incident light intensity upon a single pixel is plotted in Figure 10b. When the device was exposed to incident light through a "T"-shaped mask, the irradiated light profile was successfully obtained through an electronic readout (Figure 10c). In addition, as the absorption peak of the adopted organic photodiodes covers the green band of the light spectrum, X-ray imaging was indirectly achieved by placing a GOS scintillator film on top of the flexible imagers, which converts incident X-rays into green light (Figure 10d). Figure 10e shows a log–log plot of the measured current of a single pixel as a function of the incident X-ray dose rate. The lower limit for the linear correlation is down to ca. 10 mGy s^{-1}. As the lower limit of detection is limited by the off-current of the CNT-TFTs, lower X-ray detection limits could theoretically be obtained using such devices by tuning the electrical properties of the CNT-TFTs to obtain a lower off current. The spatial profiling of the incident X-rays can also be readily obtained using these CNT-TFT-based imagers in conjunction with the GOS films, as demonstrated in Figure 10f. These large-area visible-light imagers can serve as a new platform for the development of future interactive devices, as well as future candidates for low-cost flexible and disposable X-ray imaging devices for health applications.

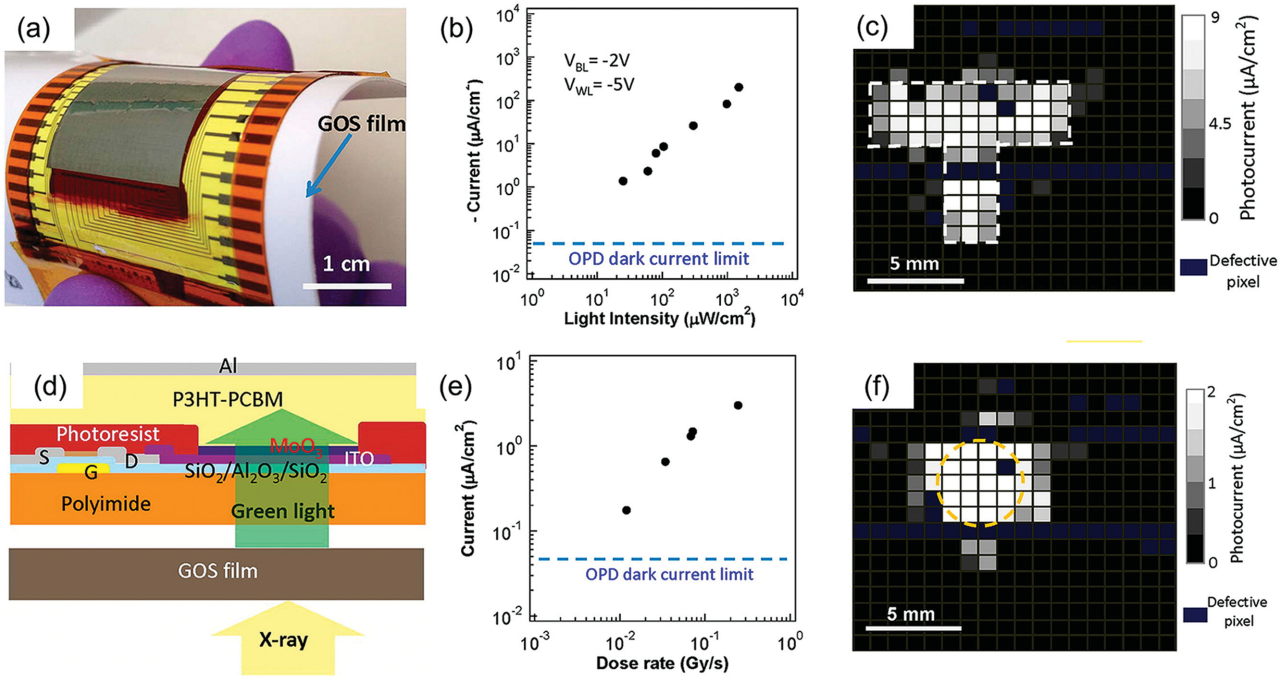

Figure 10. CNT-based TFT arrays for imaging applications. a) Optical image of a fully fabricated imager (18 × 18 pixels) placed on top of a GOS film. b) Photocurrent response of a pixel as a function of incident light intensity. c) The electronic output of the imager obtained by measuring the photocurrent of the pixels when the imager is exposed to light through a "T"-shaped shadow mask. The character "T" is readily imaged by the device. d) Cross-sectional schematic of one pixel demonstrating the X-ray sensing mechanism. X-rays are irradiated onto the GOS film, and the resulting emitted green light is detected by the OPDs of each pixel. e) Measured current from one pixel as a function of X-ray dose rate. f) Spatial mapping result of an X-ray beam with a dose rate of 100 $mGys^{-1}$. Reproduced with permission.[4] Copyright 2013, American Chemical Society.

5.4. Large-Scale Multiplexed Sensing

Moving forward, it would be desirable to be able to simultaneously map out multiple forms of stimuli using a single electronic substrate (i.e., skin). **Figure 11**a displays an optical image of an example system developed by our group, consisting of a 16 × 16 array of pixels, each integrated with a pressure, light, and temperature sensor.[136] For the pressure sensor, applied tactile pressure creates a conducting path through a laminated PSR sheet to ground. The temperature sensor utilizes a sputtered nanocrystalline InP (nc-InP) thin film contacted by interdigitated metal electrodes; as the temperature increases, the conductivity of the InP increases, leading to an increase in current. Finally, photoresponsive aSi:H is utilized as the photodetector. Two separate aSi pads are arranged in a voltage divider fashion, with one covered via metal to prevent light response, leading to a change in the divider output voltage as light intensity is increased. The output voltage is connected to the gate of a CNT-TFT for amplification of the output signal, which is, in turn, connected in series with a second CNT-TFT acting as the TFT for active-matrix backplane control. Figure 11b shows a cross-sectional schematic of the device, containing the four active layers (CNT, aSi, InP, and PSR) and four metal layers. Figure 11c, and 11d respectively show an optical image and an illustrated drawing of a single pixel within the array containing all three sensors, as well as the four CNT-TFTs used for amplification/readout. Figure 11e displays the output of the pressure sensor within a pixel, showing a minimum detectable pressure of ca. 6 kPa. Figure 11f shows the output of the temperature sensor, which has a high sensitivity of 2.6% $°C^{-1}$ below 40 °C and ca. 1.2% $°C^{-1}$ between 40 and 60 °C with minimum hysteresis, making it ideal for wearable applications for monitoring the human body temperature. In addition, the CNT-TFTs within the active-matrix backplane are relatively insensitive to temperature. Figure 11g displays the output of an a-Si photodetector, which has a light sensitivity of ca. 1.67 μA mW^{-1} cm^{-2}. In total, the array consists of 768 individual sensors and 1024 CNT-TFTs, displaying an example of the complexity that future printable CNT-based electronics may be able to achieve.

6. Outlook

Printed CNT-based flexible electronics allow for implementation of sensing, display, and interactive functionalities on flexible

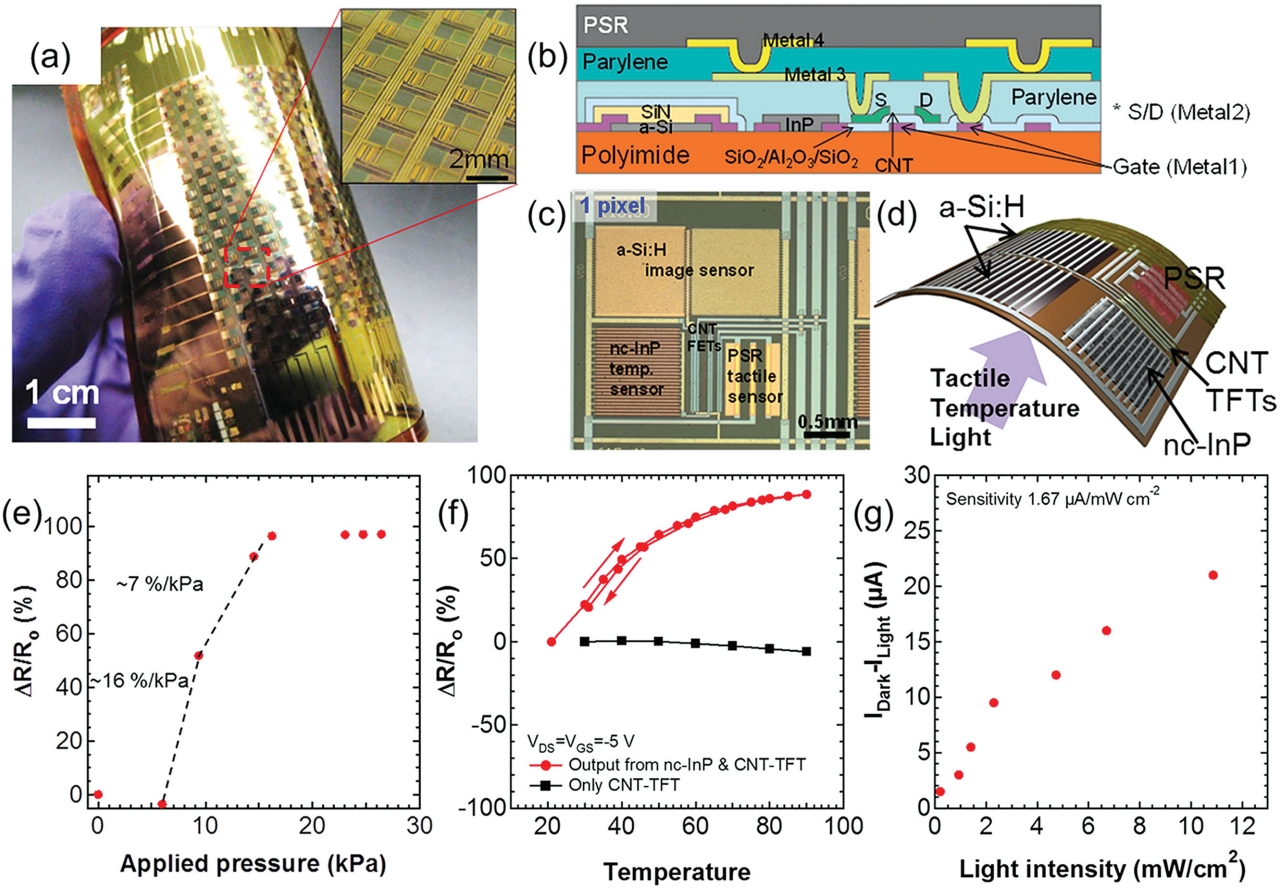

Figure 11. Large-scale multiplexed sensing arrays. a) Optical image of an electronic skin containing a 16 × 16 array of pixels capable of sensing and mapping out tactile pressure, temperature, and light intensity. b) Cross-sectional schematic of the various functional layers within the system. c,d) A zoomed-in optical image of a single pixel within the sensor array (c), along with a schematic of the direction of applied stimuli (d). e–g) Response of the sensors in a single pixel to pressure (e), temperature (f), and light (g).

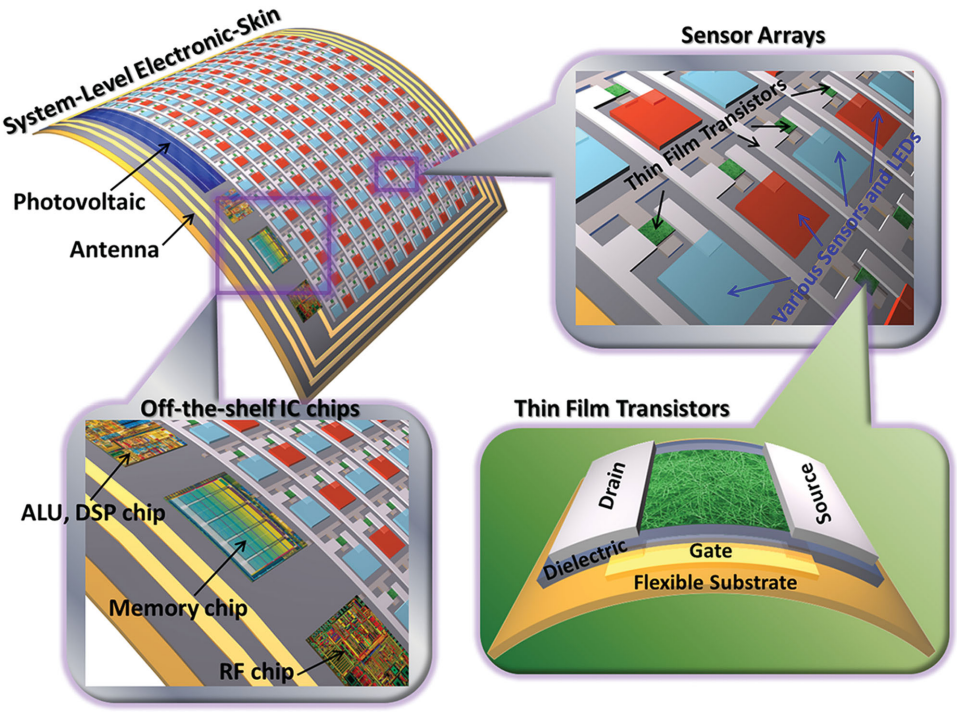

Figure 12. Image of an envisioned system-level electronic skin integrating large-area printed sensor arrays based upon CNT-TFTs with state-of-the-art commercial silicon ICs. Adapted with permission.[40] Copyright 2013, Royal Society of Chemistry.

surfaces ranging from small, disposable centimeter-squared devices up to large meter-squared functional devices. These electronics can be printed at low cost and in large volumes, and therefore can enable a wide range of possibilities in both disposable and large-area applications to further fuel the pace of integration of smart devices in our surrounding objects. Given the current state of the printed CNT-based flexible electronics technology, future efforts should primarily be shifted toward the development of fully integrated systems equipped with multifunctional pixels and sophisticated signal processing and wireless transmission. To this end, printable flexible electronics and silicon IC technologies should be synergistically combined in order to harness the unique capabilities offered by both technologies as illustrated in **Figure 12**;[40] sophisticated circuit and signal processing can be performed by the silicon IC chips, while the relatively large area smart surface is implemented by printing the flexible electronics. Additionally, the CNT sample preparation and printing process should be optimized to improve performance, yield, device-to-device variation, and resolution of the printable devices, within the context of practical manufacturing constraints, in order to ensure the widespread adoption of the technology by industry. Also, as the CNT-based devices can be significantly influenced by environmental factors such as temperature and humidity, practical system-packaging solutions must be explored to achieve robust and reproducible devices in the presence of inevitable changes in the surrounding environment. We envisage that, upon addressing the above challenges, CNT-based flexible electronics and systems will soon be one of the driving forces behind the growth of the Internet of Things.

Acknowledgements

This work was supported by the Berkeley Sensor & Actuator Center and the NSF NASCENT Center. H.O. acknowledges support from the Japan Society for the Promotion of Science (JSPS) Fellowship. K.C. acknowledges support from the Robert Noyce Memorial Fellowship in Microelectronics.

Received: October 8, 2015
Revised: December 7, 2015
Published online: February 16, 2016

[1] L. Atzori, A. Iera, G. Morabito, *Comput. Networks* **2010**, *54*, 2787.
[2] M. L. Hammock, A. Chortos, B. C.-K. Tee, J. B.-H. Tok, Z. Bao, *Adv. Mater.* **2013**, *25*, 5997.
[3] K. Takei, T. Takahashi, J. C. Ho, H. Ko, A. G. Gillies, P. W. Leu, R. S. Fearing, A. Javey, *Nat. Mater.* **2010**, *9*, 821.
[4] T. Takahashi, Z. Yu, K. Chen, D. Kiriya, C. Wang, K. Takei, H. Shiraki, T. Chen, B. Ma, A. Javey, *Nano Lett.* **2013**, *13*, 5425.
[5] C. Wang, D. Hwang, Z. Yu, K. Takei, J. Park, T. Chen, B. Ma, A. Javey, *Nat. Mater.* **2013**, *12*, 899.
[6] D.-H. Kim, N. Lu, R. Ma, Y.-S. Kim, R.-H. Kim, S. Wang, J. Wu, S. M. Won, H. Tao, A. Islam, K. J. Yu, T. Kim, R. Chowdhury, M. Ying, L. Xu, M. Li, H.-J. Chung, H. Keum, M. McCormick, P. Liu, Y.-W. Zhang, F. G. Omenetto, Y. Huang, T. Coleman, J. A. Rogers, *Science* **2011**, *333*, 838.
[7] J. Zhang, Y. Fu, C. Wang, P.-C. Chen, Z. Liu, W. Wei, C. Wu, M. E. Thompson, C. Zhou, *Nano Lett.* **2011**, *11*, 4852.
[8] C. Yeom, K. Chen, D. Kiriya, Z. Yu, G. Cho, A. Javey, *Adv. Mater.* **2015**, *27*, 1561.
[9] Y. Jung, H. Park, J.-A. Park, J. Noh, Y. Choi, M. Jung, K. Jung, M. Pyo, K. Chen, A. Javey, G. Cho, *Sci. Rep.* **2015**, *5*, 8105.

[10] H. Koo, W. Lee, Y. Choi, J. Sun, J. Bak, J. Noh, V. Subramanian, Y. Azuma, Y. Majima, G. Cho, *Sci. Rep.* **2015**, *5*, 14459.
[11] J. Noh, D. Yeom, C. Lim, H. Cha, J. Han, J. Kim, Y. Park, V. Subramanian, G. Cho, *IEEE Trans. Electron. Packag. Manuf.* **2010**, *33*, 275.
[12] H. Yao, C. Marcheselli, A. Afanasiev, I. Lahdesmaki, B. A. Parviz, in *2012 IEEE 25th Int. Conf. Micro Electro Mech. Syst. MEMS*, IEEE, Piscataway, NJ, USA **2012**, p. 769; DOI: 10.1109/MEMSYS.2012.6170299.
[13] T. Someya, Y. Kato, T. Sekitani, S. Iba, Y. Noguchi, Y. Murase, H. Kawaguchi, T. Sakurai, *Proc. Natl. Acad. Sci. USA* **2005**, *102*, 12321.
[14] T. Someya, T. Sekitani, S. Iba, Y. Kato, H. Kawaguchi, T. Sakurai, *Proc. Natl. Acad. Sci. USA* **2004**, *101*, 9966.
[15] Q. Cao, H. Kim, N. Pimparkar, J. P. Kulkarni, C. Wang, M. Shim, K. Roy, M. A. Alam, J. A. Rogers, *Nature* **2008**, *454*, 495.
[16] C. Wang, J.-C. Chien, K. Takei, T. Takahashi, J. Nah, A. M. Niknejad, A. Javey, *Nano Lett.* **2012**, *12*, 1527.
[17] K. Nomura, H. Ohta, A. Takagi, T. Kamiya, M. Hirano, H. Hosono, *Nature* **2004**, *432*, 488.
[18] Y. Sun, J. A. Rogers, *Adv. Mater.* **2007**, *19*, 1897.
[19] P. H. Lau, K. Takei, C. Wang, Y. Ju, J. Kim, Z. Yu, T. Takahashi, G. Cho, A. Javey, *Nano Lett.* **2013**, *13*, 3864.
[20] M. C. LeMieux, M. Roberts, S. Barman, Y. W. Jin, J. M. Kim, Z. Bao, *Science* **2008**, *321*, 101.
[21] H. Kang, R. Kitsomboonloha, K. Ulmer, L. Stecker, G. Grau, J. Jang, V. Subramanian, *Org. Electron.* **2014**, *15*, 3639.
[22] J. Li, L. Hu, L. Wang, Y. Zhou, G. Grüner, T. J. Marks, *Nano Lett.* **2006**, *6*, 2472.
[23] D. J. Lipomi, M. Vosgueritchian, B. C.-K. Tee, S. L. Hellstrom, J. A. Lee, C. H. Fox, Z. Bao, *Nat. Nanotechnol.* **2011**, *6*, 788.
[24] A. Chortos, G. I. Koleilat, R. Pfattner, D. Kong, P. Lin, R. Nur, T. Lei, H. Wang, N. Liu, Y.-C. Lai, M.-G. Kim, J. W. Chung, S. Lee, Z. Bao, *Adv. Mater.* **2015**, DOI:10.1002/adma.201501828.
[25] T. Sekitani, H. Nakajima, H. Maeda, T. Fukushima, T. Aida, K. Hata, T. Someya, *Nat. Mater.* **2009**, *8*, 494.
[26] T. Sekitani, Y. Noguchi, K. Hata, T. Fukushima, T. Aida, T. Someya, *Science* **2008**, *321*, 1468.
[27] D. Zhang, K. Ryu, X. Liu, E. Polikarpov, J. Ly, M. E. Tompson, C. Zhou, *Nano Lett.* **2006**, *6*, 1880.
[28] V. K. Sangwan, R. P. Ortiz, J. M. P. Alaboson, J. D. Emery, M. J. Bedzyk, L. J. Lauhon, T. J. Marks, M. C. Hersam, *ACS Nano* **2012**, *6*, 7480.
[29] C. Wang, J. Zhang, K. Ryu, A. Badmaev, L. G. De Arco, C. Zhou, *Nano Lett.* **2009**, *9*, 4285.
[30] S. Iijima, *Nature* **1991**, *354*, 56.
[31] S. Iijima, T. Ichihashi, *Nature* **1993**, *363*, 603.
[32] D. S. Bethune, C. H. Klang, M. S. de Vries, G. Gorman, R. Savoy, J. Vazquez, R. Beyers, *Nature* **1993**, *363*, 605.
[33] E. T. Thostenson, Z. Ren, T.-W. Chou, *Compos. Sci. Technol.* **2001**, *61*, 1899.
[34] P. Avouris, Z. Chen, V. Perebeinos, *Nat. Nanotechnol.* **2007**, *2*, 605.
[35] *Carbon Nanotubes*, (Eds: A. Jorio, G. Dresselhaus, M. S. Dresselhaus), Springer, Berlin/Heidelberg, Germany **2008**.
[36] A. Javey, J. Guo, Q. Wang, M. Lundstrom, H. Dai, *Nature* **2003**, *424*, 654.
[37] M. F. L. D. Volder, S. H. Tawfick, R. H. Baughman, A. J. Hart, *Science* **2013**, *339*, 535.
[38] S. Park, M. Vosguerichian, Z. Bao, *Nanoscale* **2013**, *5*, 1727.
[39] Q. Cao, J. A. Rogers, *Adv. Mater.* **2009**, *21*, 29.
[40] C. Wang, K. Takei, T. Takahashi, A. Javey, *Chem. Soc. Rev.* **2013**, *42*, 2592.
[41] T. Dürkop, B. M. Kim, M. S. Fuhrer, *J. Phys.: Condens. Matter* **2004**, *16*, R553.
[42] *Carbon Nanotube Electronics*, (Eds: J. Kong, A. Javey), Springer US, Boston, MA, USA **2009**.
[43] R. Saito, M. Fujita, G. Dresselhaus, M. S. Dresselhaus, *Appl. Phys. Lett.* **1992**, *60*, 2204.
[44] A. R. Harutyunyan, G. Chen, T. M. Paronyan, E. M. Pigos, O. A. Kuznetsov, K. Hewaparakrama, S. M. Kim, D. Zakharov, E. A. Stach, G. U. Sumanasekera, *Science* **2009**, *326*, 116.
[45] L. Ding, A. Tselev, J. Wang, D. Yuan, H. Chu, T. P. McNicholas, Y. Li, J. Liu, *Nano Lett.* **2009**, *9*, 800.
[46] H. Li, Q. Li, in *Electron. Prop. Carbon Nanotub.* (Ed.: J. M. Marulanda), InTech, Rijeka, Croatia **2011**.
[47] K. Moshammer, F. Hennrich, M. M. Kappes, *Nano Res.* **2009**, *2*, 599.
[48] H. Liu, D. Nishide, T. Tanaka, H. Kataura, *Nat. Commun.* **2011**, *2*, 309.
[49] M. S. Arnold, A. A. Green, J. F. Hulvat, S. I. Stupp, M. C. Hersam, *Nat. Nanotechnol.* **2006**, *1*, 60.
[50] S. Ghosh, S. M. Bachilo, R. B. Weisman, *Nat. Nanotechnol.* **2010**, *5*, 443.
[51] A. Ortiz-Acevedo, H. Xie, V. Zorbas, W. M. Sampson, A. B. Dalton, R. H. Baughman, R. K. Draper, I. H. Musselman, G. R. Dieckmann, *J. Am. Chem. Soc.* **2005**, *127*, 9512.
[52] A. L. Antaris, J.-W. T. Seo, A. A. Green, M. C. Hersam, *ACS Nano* **2010**, *4*, 4725.
[53] H. Li, B. Zhou, Y. Lin, L. Gu, W. Wang, K. A. S. Fernando, S. Kumar, L. F. Allard, Y.-P. Sun, *J. Am. Chem. Soc.* **2004**, *126*, 1014.
[54] F. Wang, K. Matsuda, A. F. M. M. Rahman, X. Peng, T. Kimura, N. Komatsu, *J. Am. Chem. Soc.* **2010**, *132*, 10876.
[55] R. M. Tromp, A. Afzali, M. Freitag, D. B. Mitzi, Z. Chen, *Nano Lett.* **2008**, *8*, 469.
[56] S.-Y. Ju, J. Doll, I. Sharma, F. Papadimitrakopoulos, *Nat. Nanotechnol.* **2008**, *3*, 356.
[57] A. Nish, J.-Y. Hwang, J. Doig, R. J. Nicholas, *Nat. Nanotechnol.* **2007**, *2*, 640.
[58] F. Chen, B. Wang, Y. Chen, L.-J. Li, *Nano Lett.* **2007**, *7*, 3013.
[59] X. Tu, S. Manohar, A. Jagota, M. Zheng, *Nature* **2009**, *460*, 250.
[60] M. Zheng, A. Jagota, E. D. Semke, B. A. Diner, R. S. Mclean, S. R. Lustig, R. E. Richardson, N. G. Tassi, *Nat. Mater.* **2003**, *2*, 338.
[61] E. J. F. Carvalho, M. C. dos Santos, *ACS Nano* **2010**, *4*, 765.
[62] B. S. Flavel, M. M. Kappes, R. Krupke, F. Hennrich, *ACS Nano* **2013**, *7*, 3557.
[63] X. Tu, M. Zheng, *Nano Res.* **2008**, *1*, 185.
[64] H. Liu, T. Tanaka, Y. Urabe, H. Kataura, *Nano Lett.* **2013**, *13*, 1996.
[65] D. Kiriya, K. Chen, H. Ota, Y. Lin, P. Zhao, Z. Yu, T. Ha, A. Javey, *J. Am. Chem. Soc.* **2014**, *136*, 11188.
[66] S. Kumar, J. Y. Murthy, M. A. Alam, *Phys. Rev. Lett.* **2005**, *95*, 066802.
[67] H. Park, A. Afzali, S.-J. Han, G. S. Tulevski, A. D. Franklin, J. Tersoff, J. B. Hannon, W. Haensch, *Nat. Nanotechnol.* **2012**, *7*, 787.
[68] S. Park, G. Pitner, G. Giri, J. H. Koo, J. Park, K. Kim, H. Wang, R. Sinclair, H.-S. P. Wong, Z. Bao, *Adv. Mater.* **2015**, *27*, 2656.
[69] H. Wang, P. Wei, Y. Li, J. Han, H. R. Lee, B. D. Naab, N. Liu, C. Wang, E. Adijanto, B. C.-K. Tee, S. Morishita, Q. Li, Y. Gao, Y. Cui, Z. Bao, *Proc. Natl. Acad. Sci. USA* **2014**, *111*, 4776.
[70] J. Zhang, C. Wang, C. Zhou, *ACS Nano* **2012**, *6*, 7412.
[71] M. Jung, J. Kim, J. Noh, N. Lim, C. Lim, G. Lee, J. Kim, H. Kang, K. Jung, A. D. Leonard, J. M. Tour, G. Cho, *IEEE Trans. Electron Devices* **2010**, *57*, 571.
[72] M. Ha, Y. Xia, A. A. Green, W. Zhang, M. J. Renn, C. H. Kim, M. C. Hersam, C. D. Frisbie, *ACS Nano* **2010**, *4*, 4388.
[73] J. Noh, M. Jung, K. Jung, G. Lee, J. Kim, S. Lim, D. Kim, Y. Choi, Y. Kim, V. Subramanian, G. Cho, *IEEE Electron Device Lett.* **2011**, *32*, 638.
[74] G. Grau, R. Kitsomboonloha, S. L. Swisher, H. Kang, V. Subramanian, *Adv. Funct. Mater.* **2014**, *24*, 5067.

[75] X. Yin, S. Kumar, *Chem. Eng. Sci.* **2006**, *61*, 1146.
[76] J. Vaillancourt, H. Zhang, P. Vasinajindakaw, H. Xia, X. Lu, X. Han, D. C. Janzen, W.-S. Shih, C. S. Jones, M. Stroder, M. Y. Chen, H. Subbaraman, R. T. Chen, U. Berger, M. Renn, *Appl. Phys. Lett.* **2008**, *93*, 243301.
[77] H. Okimoto, T. Takenobu, K. Yanagi, Y. Miyata, H. Shimotani, H. Kataura, Y. Iwasa, *Adv. Mater.* **2010**, *22*, 3981.
[78] P. Chen, Y. Fu, R. Aminirad, C. Wang, J. Zhang, K. Wang, K. Galatsis, C. Zhou, *Nano Lett.* **2011**, *11*, 5301.
[79] P. Calvert, *Chem. Mater.* **2001**, *13*, 3299.
[80] M. Singh, H. M. Haverinen, P. Dhagat, G. E. Jabbour, *Adv. Mater.* **2010**, *22*, 673.
[81] V. Subramanian, J. B. Chang, A. de la Fuente Vornbrock, D. C. Huang, L. Jagannathan, F. Liao, B. Mattis, S. Molesa, D. R. Redinger, D. Soltman, S. K. Volkman, Q. Zhang, in *2008 34th Eur.Solid-State Circuits Conf.*, IEEE, Piscataway, NJ, USA **2008**, p. 17; DOI: 10.1109/ESSCIRC.2008.4681785.
[82] E. Sachs, M. Cima, P. Williams, D. Brancazio, J. Cornie, *J. Eng. Ind.* **1992**, *114*, 481.
[83] J. A. Sadie, V. Subramanian, *Adv. Funct. Mater.* **2014**, *24*, 6834.
[84] T. Takahashi, K. Takei, A. G. Gillies, R. S. Fearing, A. Javey, *Nano Lett.* **2011**, *11*, 5408.
[85] K.-Y. Chun, Y. Oh, J. Rho, J.-H. Ahn, Y.-J. Kim, H. R. Choi, S. Baik, *Nat. Nanotechnol.* **2010**, *5*, 853.
[86] E. Artukovic, M. Kaempgen, D. S. Hecht, S. Roth, G. Grüner, *Nano Lett.* **2005**, *5*, 757.
[87] G. Gruner, *J. Mater. Chem.* **2006**, *16*, 3533.
[88] F. N. Ishikawa, H. Chang, K. Ryu, P. Chen, A. Badmaev, L. Gomez De Arco, G. Shen, C. Zhou, *ACS Nano* **2009**, *3*, 73.
[89] J. Noh, K. Jung, J. Kim, S. Kim, S. Cho, G. Cho, *IEEE Electron Device Lett.* **2012**, *33*, 1574.
[90] J. Zhang, C. Wang, Y. Fu, Y. Che, C. Zhou, *ACS Nano* **2011**, *5*, 3284.
[91] L. Suriyasena Liyanage, X. Xu, G. Pitner, Z. Bao, H.-S. P. Wong, *Nano Lett.* **2014**, *14*, 1884.
[92] N. Moriyama, Y. Ohno, T. Kitamura, S. Kishimoto, T. Mizutani, *Nanotechnology* **2010**, *21*, 165201.
[93] T.-J. Ha, K. Chen, S. Chuang, K. M. Yu, D. Kiriya, A. Javey, *Nano Lett.* **2014**, *15*, 392.
[94] Z. Zhang, X. Liang, S. Wang, K. Yao, Y. Hu, Y. Zhu, Q. Chen, W. Zhou, Y. Li, Y. Yao, J. Zhang, L.-M. Peng, *Nano Lett.* **2007**, *7*, 3603.
[95] L. Ding, S. Wang, Z. Zhang, Q. Zeng, Z. Wang, T. Pei, L. Yang, X. Liang, J. Shen, Q. Chen, R. Cui, Y. Li, L.-M. Peng, *Nano Lett.* **2009**, *9*, 4209.
[96] C. Zhou, J. Kong, E. Yenilmez, H. Dai, *Science* **2000**, *290*, 1552.
[97] A. Javey, R. Tu, D. B. Farmer, J. Guo, R. G. Gordon, H. Dai, *Nano Lett.* **2005**, *5*, 345.
[98] M. Shim, A. Javey, N. W. Kam, H. Dai, *J. Am. Chem. Soc.* **2001**, *123*, 11512.
[99] P. Qi, O. Vermesh, M. Grecu, A. Javey, Q. Wang, H. Dai, S. Peng, K. J. Cho, *Nano Lett.* **2003**, *3*, 347.
[100] N. Chimot, V. Derycke, M. F. Goffman, J. P. Bourgoin, H. Happy, G. Dambrine, *Appl. Phys. Lett.* **2007**, *91*, 153111.
[101] J. Zaumseil, *Semicond. Sci. Technol.* **2015**, *30*, 074001.
[102] Y. Sun, H. H. Wang, *Adv. Mater.* **2007**, *19*, 2818.
[103] Y. Sun, H. H. Wang, *Appl. Phys. Lett.* **2007**, *90*, 213107.
[104] S. Mubeen, T. Zhang, B. Yoo, M. A. Deshusses, N. V. Myung, *J. Phys. Chem. C* **2007**, *111*, 6321.
[105] J. Sippel-Oakley, H.-T. Wang, B. S. Kang, Z. Wu, F. Ren, A. G. Rinzler, S. J. Pearton, *Nanotechnology* **2005**, *16*, 2218.
[106] J. Li, Y. Lu, Q. Ye, M. Cinke, J. Han, M. Meyyappan, *Nano Lett.* **2003**, *3*, 929.
[107] E. Bekyarova, M. Davis, T. Burch, M. E. Itkis, B. Zhao, S. Sunshine, R. C. Haddon, *J. Phys. Chem. B* **2004**, *108*, 19717.
[108] T. Zhang, M. B. Nix, B.-Y. Yoo, M. A. Deshusses, N. V. Myung, *Electroanalysis* **2006**, *18*, 1153.
[109] P. Young, Y. Lu, R. Terrill, J. Li, *J. Nanosci. Nanotechnol.* **2005**, *5*, 1509.
[110] D. Fu, H. Lim, Y. Shi, X. Dong, S. G. Mhaisalkar, Y. Chen, S. Moochhala, L.-J. Li, *J. Phys. Chem. C* **2008**, *112*, 650.
[111] B. Philip, J. K. Abraham, A. Chandrasekhar, V. K. Varadan, *Smart Mater. Struct.* **2003**, *12*, 935.
[112] M. D. Shirsat, T. Sarkar, J. Kakoullis, N. V. Myung, B. Konnanath, A. Spanias, A. Mulchandani, *J. Phys. Chem. C* **2012**, *116*, 3845.
[113] P.-C. Chen, S. Sukcharoenchoke, K. Ryu, L. Gomez de Arco, A. Badmaev, C. Wang, C. Zhou, *Adv. Mater.* **2010**, *22*, 1900.
[114] J. P. Novak, E. S. Snow, E. J. Houser, D. Park, J. L. Stepnowski, R. A. McGill, *Appl. Phys. Lett.* **2003**, *83*, 4026.
[115] K. Cattanach, R. D. Kulkarni, M. Kozlov, S. K. Manohar, *Nanotechnology* **2006**, *17*, 4123.
[116] S. N. Kim, J. F. Rusling, F. Papadimitrakopoulos, *Adv. Mater.* **2007**, *19*, 3214.
[117] M. Lu, D. Lee, W. Xue, T. Cui, *Sens. Actuators, A* **2009**, *150*, 280.
[118] X. Tang, S. Bansaruntip, N. Nakayama, E. Yenilmez, Y. Chang, Q. Wang, *Nano Lett.* **2006**, *6*, 1632.
[119] D. R. Kauffman, A. Star, *Angew. Chem. Int. Ed.* **2008**, *47*, 6550.
[120] T. Zhang, S. Mubeen, N. V. Myung, M. A. Deshusses, *Nanotechnology* **2008**, *19*, 332001.
[121] K. Parikh, K. Cattanach, R. Rao, D.-S. Suh, A. Wu, S. K. Manohar, *Sens. Actuators, B* **2006**, *113*, 55.
[122] P. Hu, J. Zhang, L. Li, Z. Wang, W. O'Neill, P. Estrela, *Sensors* **2010**, *10*, 5133.
[123] J. Koh, M. Yi, B. Y. Lee, T. H. Kim, J. Lee, Y. M. Jhon, S. Hong, *Nanotechnology* **2008**, *19*, 505502.
[124] J. N. Tey, I. P. M. Wijaya, Z. Wang, W. H. Goh, A. Palaniappan, S. G. Mhaisalkar, I. Rodriguez, S. Dunham, J. A. Rogers, *Appl. Phys. Lett.* **2009**, *94*, 013107.
[125] B.-S. Kim, S. W. Lee, H. Yoon, M. S. Strano, Y. Shao-Horn, P. T. Hammond, *Chem. Mater.* **2010**, *22*, 4791.
[126] M. E. Roberts, M. C. LeMieux, Z. Bao, *ACS Nano* **2009**, *3*, 3287.
[127] C. B. Jacobs, M. J. Peairs, B. J. Venton, *Anal. Chim. Acta* **2010**, *662*, 105.
[128] S. K. Vashist, D. Zheng, K. Al-Rubeaan, J. H. T. Luong, F.-S. Sheu, *Biotechnol. Adv.* **2011**, *29*, 169.
[129] M. Kaempgen, S. Roth, *J. Electroanal. Chem.* **2006**, *586*, 72.
[130] J.-Y. Lee, E.-J. Park, C.-J. Lee, S.-W. Kim, J. J. Pak, N. K. Min, *Thin Solid Films* **2009**, *517*, 3883.
[131] J.-Y. Chiu, C.-M. Yu, M.-J. Yen, L.-C. Chen, *Biosens. Bioelectron.* **2009**, *24*, 2015.
[132] X. B. Yan, X. J. Chen, B. K. Tay, K. A. Khor, *Electrochem. Commun.* **2007**, *9*, 1269.
[133] S. Sánchez, M. Pumera, E. Fàbregas, *Biosens. Bioelectron.* **2007**, *23*, 332.
[134] D. Sun, M. Y. Timmermans, Y. Tian, A. G. Nasibulin, E. I. Kauppinen, S. Kishimoto, T. Mizutani, Y. Ohno, *Nat. Nanotechnol.* **2011**, *6*, 156.
[135] Z. Yu, X. Niu, Z. Liu, Q. Pei, *Adv. Mater.* **2011**, *23*, 3989.
[136] K. Takei, K. Chen, A. Javey, unpublished.